

The HRX-BL Lac sample - evolution of BL Lac objects

V. Beckmann^{1,2,3}, D. Engels¹, N. Bade¹, and O. Wucknitz⁴

¹ Hamburger Sternwarte, Gojenbergsweg 112, D-21029 Hamburg, Germany

² INTEGRAL Science Data Centre, Chemin d'Écogia 16, CH-1290 Versoix, Switzerland

³ Institut für Astronomie und Astrophysik, Universität Tübingen, Sand 1, D-72076 Tübingen, Germany

⁴ Universität Potsdam, Astroteilchenphysik, Am Neuen Palais 10, D-14469 Potsdam, Germany

Received date; accepted date

Abstract. The unification of X-ray and radio selected BL Lacs has been an outstanding problem in the blazar research in the past years. Recent investigations have shown that the gap between the two classes can be filled with intermediate objects and that apparently all differences can be explained by mutual shifts of the peak frequencies of the synchrotron and inverse Compton component of the emission. We study the consequences of this scheme using a new sample of X-ray selected BL Lac objects comprising 104 objects with $z < 0.9$ and a mean redshift $\bar{z} = 0.34$. 77 BL Lacs, of which the redshift could be determined for 64 (83%) objects, form a complete sample. The new data could not confirm our earlier result, drawn from a subsample, that the negative evolution vanishes below a synchrotron peak frequency $\log \nu_{\text{peak}} = 16.5$. The complete sample shows negative evolution at the 2σ level ($\langle V_e/V_a \rangle = 0.42 \pm 0.04$). We conclude that the observed properties of the HRX BL Lac sample show typical behaviour for X-ray selected BL Lacs. They support an evolutionary model, in which flat-spectrum radio quasars (FSRQ) with high energetic jets evolve towards low frequency peaked (mostly radio-selected) BL Lac objects and later on to high frequency peaked (mostly X-ray selected) BL Lacs.

Key words. BL Lacertae objects: general - X-rays: galaxies

1. Introduction

BL Lac objects are a rare type of Active Galactic Nuclei (AGN), which are observationally distinguished mainly by the absence of strong emission lines. They have strong X-ray and radio emission, and they often show strong variability and optical polarization. Their observational properties are usually explained by a particular line of sight toward the galaxy nucleus, which in BL Lacs is thought to be parallel to a jet emerging from this nucleus.

Two search strategies are commonly used to find BL Lacs. The first is a search for strong X-ray sources with a high ratio of X-ray to optical flux, yielding X-ray selected BL Lacs (XBL). The second is to search among flat spectrum radio sources to find radio selected ones (RBL). As the radio and X-ray surveys got more and more sensitive, the properties of both groups started to overlap, raising the question of how they are related. Padovani & Giommi (1995) noticed that the spectral energy distribution (quantified by $\log \nu L_\nu$) of radio and X-ray selected BL Lacs shows peaks at different frequencies, and suggested that this is the basic difference between the two classes of BL Lacs. They introduced the notation of *high-energy cutoff BL Lacs* (HBLs) and *low-energy cutoff BL*

Lacs (LBLs). Most, but not all, XBLs are HBLs, while the group of LBLs is preferentially selected in the radio region.

In general, BL Lacs are considered as part of a larger class of objects, the blazars, which have similar properties but show emission lines in addition, and for which this scenario applies as well. Ghisellini et al. (1998) proposed that the range of peak frequencies observed is governed primarily by the efficiency of radiative cooling, and that the other physical parameters strongly depend on it. They found an inverse correlation between the energy of the Lorentz factor of particles emitting at the peaks of the SED (γ_{peak}) and the energy density of the magnetic and radiation field of $\gamma_{\text{peak}} \propto U^{-0.6}$. This correlation was extended later on for low power (high peaked) BL Lacs by taking into account the finite time for the injection of particles in the jet (Ghisellini et al. 2002). Combined modelling of the time-dependent electron injection and the self consistent radiation transport in jets of high peaked blazars lead to the conclusion that differences in the appearance can be explained by either self-synchrotron or external Compton dominated processes (Böttcher & Chiang 2002). Other studies focussed on the importance of shock events in the blazar jets to explain variability on short timescales (e.g. Bicknell & Wagner 2002). Based on these models the most

important factor in the appearance of blazars seems nowadays the energy density of the jet. Maraschi & Tavecchio (2002) showed that this energy density is related to the accretion rate in the AGN disk and proposed that all blazar types have similar black hole masses but that the low power blazars exhibit lower accretion rates.

Unlike all other AGNs, and different from RBLs also, the space density or the luminosity of XBLs showed an increase with time (e.g. Rector et al. 2000). This is called negative evolution. Bade et al. (1998) probed this property with a new ROSAT selected XBL sample and confirmed the negative evolution only for extreme XBLs, e.g. HBLs with very high energy cutoffs ($\log \nu_{\text{peak}} > 16.5$). The result for less extreme XBLs, called intermediate-energy cutoff BL Lacs (IBLs) by Bade et al., was compatible with no evolution. This difference in evolutionary behaviour indicated the presence of a smooth transition between HBLs and LBLs. However, these findings were based on only 39 BL Lacs, prompting us to increase the size of this sample considerably. The results of this effort, the HRX-BL Lac sample presented here, comprises now 77 BL Lacs and is the largest complete XBL sample so far.

Recent models tried to explain the different evolutionary behaviour of HBLs and LBLs by assuming that BL Lacs start as LBLs and evolve into HBLs as they grow older (Georganopoulos & Marscher 1998, Cavaliere & D’Elia 2002). As described by e.g. Padovani & Urry the spectral energy distributions (SED) of BL Lacs are characterized by two components, both consisting of beamed continuum emission from the plasma of the jets. The first component is synchrotron emission, peaking in the mm to far IR for LBLs. The second component is inverse Compton (IC) emission peaking at MeV energies. HBLs have SEDs peaking in the keV and in the GeV-TeV band respectively. A decrease of power of the jets during the BL Lac evolution would then be accompanied by an increase of the peak frequencies and accordingly a transformation of the LBLs into HBLs (Georganopoulos & Marscher 1998). This model is in fact valid for the whole blazar class: BL Lacs in general show lower power and beaming factors than the Flat Spectrum Radio Quasars (FSRQs), as revealed by e.g. Madau et al. (1987), Padovani (1992), Ghisellini et al. (1993). It naturally explains the different evolution, which is slightly negative for HBLs, slightly positive for LBLs, and clearly positive for the FSRQ/blazar class. This model explains the different types of BL Lac objects only by different global intrinsic power (Maraschi & Rovetti 1994), and not by a different viewing angle. Nevertheless different orientation is probably important as secondary effect necessary to explain the large scatter of observed quantities.

The HRX-BL Lac sample contributes to the discussion with a large and complete sample of X-ray selected BL Lac objects. Previous studies (e.g. Fossati et al. 1998) used a compilation of different BL Lac surveys, like the X-ray selected EMSS (Stocke et al. 1991, Rector et al. 2000), the radio selected 1 Jy BL Lac sample (Stickel et al. 1991, Rector & Stocke 2001), and a FSRQ sample de-

Table 1. Boundaries of the selection area.

Boundaries (J2000.0)		Area [deg ²]
α	δ	
$7^{\text{h}} \leq \alpha < 8^{\text{h}}$	$30^{\circ} < \delta < 85^{\circ}$	426
$8^{\text{h}} \leq \alpha < 12^{\text{h}}$	$20^{\circ} < \delta < 85^{\circ}$	2248
$12^{\text{h}} \leq \alpha < 14^{\text{h}}$	$20^{\circ} < \delta < 65^{\circ}$	970
$14^{\text{h}} \leq \alpha \leq 16^{\text{h}}$	$20^{\circ} < \delta < 85^{\circ}$	1124

rived from the 2 Jy radio sample of Wall & Peacock (1985) to investigate the overall picture of the blazar class, ranging from the FSRQs to the BL Lac objects. In contrast to this the HRX-BL Lac survey is concentrating on a blazar subclass, the HBL and IBLs, and is homogeneous in having the same selection criteria for all objects, making it comparable with the REX-survey (Maccacaro et al. 1998, Caccianiga et al. 1999), the DRXBS (Perlman et al. 1998, Landt et al. 2002), and the sedentary multifrequency BL Lac sample (Giommi, Menna, & Padovani 1999).

We will describe our selection method of BL Lac candidates in Section 2 and the results of the identification process using literature data and own observations in Section 3. The spectral energy distribution of the HRX-BL Lac sample is analyzed in Section 4, where we demonstrate that for the HBL class the knowledge about the X-ray and optical flux is sufficient to determine the peak frequency of the synchrotron branch. The spatial distribution of the sample is described in Section 5. We conclude with a discussion of the compatibility of the results from the HRX BL Lac sample with recent studies.

Throughout the article a cosmology with $H_0 = 50 \text{ km sec}^{-1} \text{ Mpc}^{-1}$ and a deceleration parameter $q_0 = 0.5$, assuming a Friedmann universe with $\Lambda = 0$, has been used.

2. BL Lac candidate selection

In the beginning the HRX-BL Lac sample originated from the Hamburg-RASS Bright X-ray AGN sample (HRX), which was created by identification of the ROSAT All-Sky Survey (RASS) with the aid of objective prism plates of the Hamburg Quasar Survey (HQS; Hagen et al. 1995). The BL Lac subsample was selected on an area of 1687 deg^2 with a count-rate limit of $hcps \geq 0.075 \text{ sec}^{-1}$ and on additional 1150 deg^2 with a limit of $hcps \geq 0.15 \text{ sec}^{-1}$. This sample was analyzed by Bade et al. (1998) and is referred here as the HRX-BL Lac *core sample*. It consists of 39 BL Lacs, 34 of which are also part of the present sample.

The fraction of BL Lacs in the HRX was $\sim 10\%$. Therefore, an increase of the sample size based on optical identification alone is rather inefficient. This can be alleviated using radio information, as all BL Lacs from the core sample were detected as radio sources in the NRAO VLA Sky Survey (NVSS, Condon et al. 1998). Also, to the authors knowledge, all known BL Lac objects do have radio counterparts down to the $\sim 2.5 \text{ mJy}$ level, which

is similar to the detection limit of the NVSS. We concluded therefore that for the high X-ray count-rates used we can include radio detection in the NVSS as selection criterium without loosing BL Lac objects. As X-ray input we used the ROSAT Bright Source Catalog (RASS-BSC; Voges et al. 1999) with a count-rate limit (0.5–2.0 keV) of $hcps \geq 0.09 \text{ sec}^{-1}$. We cross-correlated this catalogue with the NVSS adopting an error circle of $30''$ around the X-ray position. We extended the sky area studied to 4768 deg^2 encompassing the area of 2837 deg^2 studied by Bade et al. (1998), and we applied a unique limit of $hcps \geq 0.09 \text{ sec}^{-1}$. The boundaries of the area are given in Table 1.

The cross-correlation yielded 223 matches between X-ray and radio sources. The complete list of these objects is given in Table 8 (page 18). The coordinates listed are the X-ray positions (J2000.0). More than 99.9% of the sources have a positioning error $\Delta \leq 25''$ (Voges et al. 1999). The column “Name” lists alternative names to the ROSAT designation, when available. Redshifts and classification are taken from the NED or SIMBAD database or were determined on the base of own follow-up observations. All objects, for which we obtained own data are marked.

The cross correlation might be incomplete for lobe-dominated radio sources, as in those cases the radio emission will consist of more than one component offset from the X-ray position. However, for none of the X-Ray BSC sources we found multiple radio sources within the search radius, and as BL Lacs are core-dominated radio sources no selection biases are expected.

3. Classification of BL Lac candidates

3.1. Results from NED and SIMBAD database queries

The 223 candidates were classified in a two-step process. First we searched for known optical counterparts in the NASA/IPAC Extragalactic Database (NED)¹ and in the SIMBAD² database. Special care was taken to avoid confusion of BL Lac objects with normal galaxies and other types of AGNs. A database entry of an object as “galaxy” without spectroscopic information was not accepted as an identification, because nearby BL Lac objects in elliptical galaxies might not have been recognized. For galaxies with redshift information and for objects with “AGN” or “QSO” identification but without additional information (e.g. redshift) the original literature was consulted before the object was dismissed as BL Lac.

In total 101 objects could be classified this way.³ Of the remaining objects a few candidates were classified as stars on the objective prism plates of the HQS, and another

¹ The NED is operated by the Jet Propulsion Laboratory, California Institute of Technology, under contract with the National Aeronautics and Space Administration.

² The SIMBAD Astronomical Database is operated by the Centre de Données astronomiques de Strasbourg.

³ at the time of writing this paper, already 205 of the objects have a classification in the NED

Table 2. Spectroscopic follow-up observation runs. The last column gives the number of objects observed. Some of the objects were observed several times.

Telescope & Instrument	Date	#nights	N^b
3.5m Calar Alto (MOSCA)	March 1997	4	30
WHT / La Palma (ISIS)	April 1997	2	19
3.5m Calar Alto (MOSCA)	Feb. 1998	6	89
3.5m Calar Alto (MOSCA)	Feb. 1999	$\sim 1^a$	9

^a morning and evening hours of three nights.

^b number of objects observed in this observation run.

few as obvious clusters of galaxies based on direct plates and on the fact that these sources show extended X-ray emission. For all other candidates follow-up observations were obtained.

3.2. Observations of the remaining unclassified BL Lac candidates

Spectroscopic observations to classify the remaining BL Lac candidates and to determine their redshifts were made with the 3.5m telescope on Calar Alto equipped with the multiobject spectrograph MOSCA and with the 4.2m WHT on La Palma equipped with ISIS (Table 2). Most of the results from the 1997 observation runs have already been presented in Bade et al. (1998). For the classification with MOSCA, we used the G500 grism, which covers a wavelength range 4250 – 8400 Å with a pixel-to-pixel resolution of 12 Å. If necessary, additional spectra were taken with the G1000 and R1000 grisms to determine redshifts. These spectra have a resolution of 6 Å and cover the ranges 4400–6600 Å and 5900–8000 Å respectively. The spectra were reduced in a standard way: bias subtraction, flat-field correction using morning and evening skyflats, and response determination of the detector using spectrophotometric standard stars. BL Lac objects by definition have no or very weak emission lines. Integration times of $\approx 1000 \dots 2000 \text{ sec}$ were needed to detect the weak absorption lines of the host galaxy, which is often out-shined by the non-thermal continuum of the point-like central synchrotron source. Most observations were made under non-photometric conditions.

Optical photometry in the Johnson B band has been obtained for many of the optically faint BL Lacs with the Calar Alto 1.23m telescope (Beckmann 2000a). Especially for several of the very faint objects ($B > 20 \text{ mag}$) no reliable photometry was available before. For these objects we have now optical magnitudes with an error of $\Delta B \leq 0.1 \text{ mag}$. For the other objects the acquisition frames of the spectroscopic runs have been used to determine a B magnitude, or values from the literature have been taken. For the brighter objects ($B < 18 \text{ mag}$) also the HQS calibrated objective prism plates have been used, which have an error of $\Delta B \leq 0.3 \text{ mag}$.

Table 3. Summary of identifications of objects from the BSC/NVSS correlation (cf. Table 8)

object type	total number	fraction
BL Lac	77	34.5%
Seyfert 1	65	29.1%
Seyfert 2	8	3.6%
Quasar	6	2.7%
blazar	2	0.9%
LINER	5	2.2%
Galaxy cluster	29	13.0%
Galaxies	19	8.5%
Stars	8	3.6%
SNR	2	0.9%
Unidentified	2	0.9%
Total	223	

3.3. Results from follow-up observations

Follow-up observations were made of 117 objects, including the unidentified candidates from the BSC/NVSS correlation and additionally a number of objects, which were considered to be promising BL Lac candidates, but did not match the selection criteria described before (e.g. too low X-ray count rate). In total we discovered 53 BL Lac objects according to the classification criteria, which are discussed in Section 3.4. As a considerable number of the objects was discovered independently by other groups in the meantime, we are left over with 26 new BL Lacs: 11 from the BSC/NVSS correlation and 15 from the additionally observed objects.

3.3.1. The complete HRX BL Lac sample

The 11 new BL Lac objects discovered among the objects from the BSC/NVSS correlation are marked in Table 8 and their spectra are included in Figure 8. Based on our spectra we could confirm or revise redshifts for several other BL Lac objects. Five objects from this correlation with other identifications than BL Lac and without NED or SIMBAD entry so far, are marked in Table 8 in addition.

Summarizing, the optical identification of the 223 BSC/NVSS objects leads to the following distribution of object classes within the radio/X-ray correlation (Table 3): 35% are BL Lac objects, 36% are other AGNs (QSO, Seyfert 1/2, FSRQs), 11% galaxies (including starburst galaxies and LINERs), 13% cluster of galaxies, and 4% stars (including 2 supernova remnants). Only a fraction of 1% of the 223 candidates is yet not identified.

The 77 BL Lacs from the BSC/NVSS correlation are called the *complete HRX BL Lac sample*. In comparison to the EMSS BL Lac sample, this sample probes a population of objects with lower α_{RO} and α_{OX} values and contains therefore more radio quiet and stronger X-ray dominated objects. The HRX-BL Lac sample is the largest complete sample of X-ray selected BL Lac objects. Table 4 compares

the HRX BL Lac sample with four other X-ray selected BL Lac Surveys: the EMSS based sample (ReCTOR et al. 2000), the sample by Laurent-Muehleisen et al. (1999) based on the correlation of the RASS with the Green Bank radio survey, the REX survey using the NVSS in combination with the sources found in the ROSAT pointed observations (Caccianiga et al. 1999), and the DXRBS (Perlman et al. 1998), which uses the ROSAT data base WGACAT and PMN/NVSS radio data.

3.3.2. The extended HRX BL Lac sample

Among the BL Lac candidates observed additionally we could confirm another 27 BL Lac objects, from which 15 did not appear in the literature so far. Together with the 77 BL Lacs from the complete sample they form the *extended HRX BL Lac sample* comprising 104 objects. The spectra of the 15 new BL Lacs are presented in Figure 8 together with the 12 new BL Lacs from the complete sample. The spectra of all other objects including those from objects not identified as BL Lacs will be accessible on the web⁴.

The properties of the 104 BL Lacs of the extended sample are presented in Table 9 (page 20). The BL Lacs discovered additionally are marked by an asterisk and the new BL Lacs are labeled by “new”. This Table lists the object names, the NVSS radio coordinates (J2000.0), redshifts, ROSAT PSPC (0.5 - 2.0 keV) X-ray fluxes in 10^{-12} erg cm⁻² sec⁻¹, 1.4 GHz radio fluxes in mJy from the NVSS radio catalogue, B magnitudes, K magnitudes, and the calcium break index. The radio positions have an error of less than 5'' (for the faintest objects) and are therefore considerably more accurate than the X-ray positions given in Table 8.

The RASS-BSC fluxes have been computed by using the count rate and a single-power law with free fitted absorption N_H . The spectral slope and N_H are determined by the hardness ratios, a method described by Schartel (1994). The hardness ratio is defined as $HR = (H - S)/(H + S)$ with H and S being the number of counts in the hard and soft energy bands; typically two ratios are computed: $HR1$ with energy ranges $S = 0.1 - 0.4$ keV and $H = 0.5 - 2.0$ keV, and $HR2$ with $S = 0.5 - 0.9$ keV and $H = 1.0 - 2.0$ keV (Voges et al. 1999). The values for the hardness ratios range by definition from +1 for extremely hard to -1 for very soft X-ray spectra. The error estimate for the N_H and α_X values is based on the hardness ratios only, not on the photon spectrum itself. Therefore this method does not give χ^2 values, but is able to determine 68% (1σ) errors. This is done by exploring the hardness-ratio, spectral slope, and N_H parameter space, determining the 1σ region within it for a given set of parameter components.

The near infrared data are taken from the Two-Micron All-Sky Survey (2MASS, Skrutskie et al. 1995, Stiening et

⁴ <http://www.hs.uni-hamburg.de/bllac.html>

Table 4. Properties of the Hamburg BL Lac samples in comparison to other recent samples

sample	Reference	number of objects	X-ray limit	radio limit	optical limit
HRX core sample	Bade et al. 1998	39	0.075/0.15 sec ⁻¹ ^{a,g)}	-	-
HRX-BL Lac	this work	77	0.09 sec ⁻¹ ^{a,g)}	2.5 mJy ^{b)}	-
RGB	Laurent-Muehleisen	127	0.05 sec ⁻¹ ^{a,c)}	15 ... 24 mJy ^{d)}	18.5 mag ^{e)}
RGB complete	et al. 1999	33	0.05 sec ⁻¹ ^{c)}	15 ... 24 mJy ^{d)}	18.0 mag ^{e)}
EMSS	Rector et al. 2000	41	2 × 10 ⁻¹³ ^{f)}	-	-
REX	Caccianiga et al. 2002	55	4 × 10 ⁻¹³ ^{g)}	2.5 mJy ^{b)}	$B \leq 20.5$ mag
DXRBS	Padovani 2001	30	few × 10 ⁻¹⁴ ^{c)}	~ 50 mJy	-

^{a)} ROSAT All Sky Survey count rate limit

^{b)} NVSS radio flux limit at 1.4 GHz

^{c)} Full (0.1 – 2.4 keV) PSPC energy band.

^{d)} GB catalog flux limit at 5 GHz

^{e)} O magnitude determined from POSS-I photographic plates

^{f)} EINSTEIN IPC (0.3 – 3.5 keV) flux limit in [erg cm⁻² sec⁻¹]

^{g)} hard (0.5 – 2 keV) PSPC energy band.

al. 1995). In Table 9 only the K -magnitude is listed, but for the analysis we also used J and H from the 2MASS.

The calcium break index (Ca-break) is defined as follows (Dressler & Shectman 1987):

$$Ca - break[\%] = 100 \cdot \frac{f_{\text{upper}} - f_{\text{lower}}}{f_{\text{upper}}} \quad (1)$$

with f_{upper} and f_{lower} being the mean fluxes measured in the 3750 Å < λ < 3950 Å and 4050 Å < λ < 4250 Å objects rest frame band respectively. The measurement of the break was possible only if the redshift was known and if the break was within the spectral range covered by the observation. Therefore break values are available for 30 of the HRX-BL Lac only. In seven cases the break value is negative. This is in most cases due to a low signal to noise of the spectra. Only for one object (1RXS J111706.3+201410) the negative calcium break index is not consistent with a value of 0% and we assume that here the underlying power law of the jet emission outshines the host galaxy, so that the measured negative 'break value' is in fact based on the synchrotron component.

Figure 1 shows the redshift distribution of the HRX-BL Lac extended and complete samples. The mean redshift for the *complete* and *extended sample* are $\bar{z} = 0.31$ and $\bar{z} = 0.34$, respectively. We note that in comparison to the *core sample* no new BL Lacs with $z > 0.7$ were found, which contribute to the *complete sample*.

3.4. BL Lac classification criteria

The characterizing feature of BL Lac spectra in the optical is the presence of a non-thermal continuum which is well described by a single power law. A second component is the emission of the host galaxy, which contributes absorption features in addition to continuum emission. If the BL Lac itself shows no emission lines at all, redshift determination is only possible by identifying these absorption features. The host galaxies are in majority giant elliptical

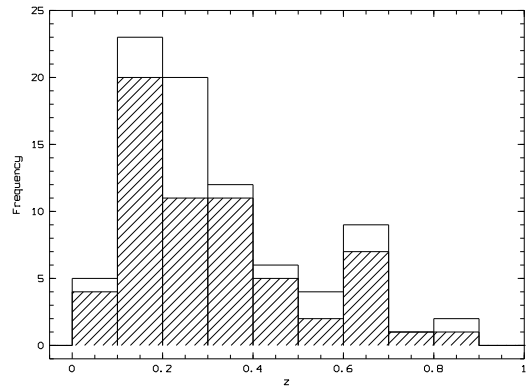


Fig. 1. Distribution of redshifts in the extended HRX-BL Lac sample. The hatched part refers to the *complete sample*.

galaxies (e.g. Urry et al. 2000), having strong absorption features caused by the stellar content.

Expected absorption features in the optical, which can be used for redshift determination, have already been discussed in detail by Bade et al. (1998). The most prominent feature in the spectra of elliptical galaxies is the so-called “calcium break” at 4000 Å. Its strength is given by the calcium break index, as defined before.

Most of the AGN with emission lines found in the radio/X-ray correlation are Seyfert type galaxies or LINER (see Table 3). These AGN do not show a calcium break. For the other objects the strength of the calcium break can be used to distinguish between normal elliptical galaxies and BL Lac objects. For the former, this contrast is $\geq 40\%$ with the higher flux to the red side of the break. Our criteria to classify BL Lac objects were defined by Bade et al. (1998) for the core sample and are spectroscopically similar to those applied to the Einstein Medium-Sensitivity Survey (EMSS; Stocke et al. 1991). However, we relaxed the upper limit for the strength of the calcium

break index from 25% to now 40% when other properties of the object were consistent with a BL Lac classification. This follows the findings of previous studies (Marchã et al. 1996; Laurent-Muehleisen et al. 1999; Rector et al. 2000) that there exist galaxies with strengths $25\% < \text{Ca-break} < 40\%$, which fulfill all other selection criteria for BL Lac objects. Explicitly the selection criteria are now:

- No emission lines with $W_\lambda > 5 \text{ \AA}$
- The contrast of the Ca II break from the host galaxy must be less than 40%.

With respect to the first criterium no misclassifications are expected as there were no objects found within the BSC/NVSS correlation with weak emission lines and equivalent widths of several 10 \AA .

Borderline cases are more likely with respect to the calcium break index, because the transition between non-active elliptical galaxies and BL Lacs is smooth. This is clearly shown in Figure 2, in which our measured break strength is plotted vs. the optical luminosity L_B , as derived in Section 4.2. Both quantities are correlated and almost evenly distributed up to Ca-break $\sim 40\%$.

The observed correlation might be affected by a varying fraction of host galaxy light included in the spectra. In nearby objects the BL Lac host galaxy might not have been fully covered by the slit and therefore the calcium break strength could have been underestimated. However, as the low-redshift objects are mainly the less luminous ones, this effect cannot explain the decreasing strength of the calcium break with increasing luminosities.

This correlation is not only seen in the optical domain, but is also present if we use radio, near infrared or X-ray luminosity instead. In all wavelength regions from the optical to the X-rays the correlation between emitted luminosity and break strength is significant. Therefore we would like to stress the point that the observed correlations are not due to observational selection effects.

Misclassifications might have been occurred also due to large errors for the measured break strengths in some of our spectra with low signal to noise ratio. However for all objects except three of the HRX-BL Lac *complete sample* the break strengths are $< 25\%$, making a misclassification unlikely. The three objects with a calcium break strength in the range $25\% < \text{Ca-break} < 40\%$ are 1ES 0927+500, 1RXS 114754.9+220548, and 1RXS 151040.8+333515 (cf. Table 9) and they were included in the sample, because they fulfill other BL Lac properties, for example strong polarization ($P > 6\%$) in the NVSS.

4. Spectral Energy Distribution

To study the spectral energy distribution (SED) of the HRX-BL Lac objects, overall spectral indices were calculated to derive general correlations within the sample. Throughout this Section the *extended sample* is analyzed.

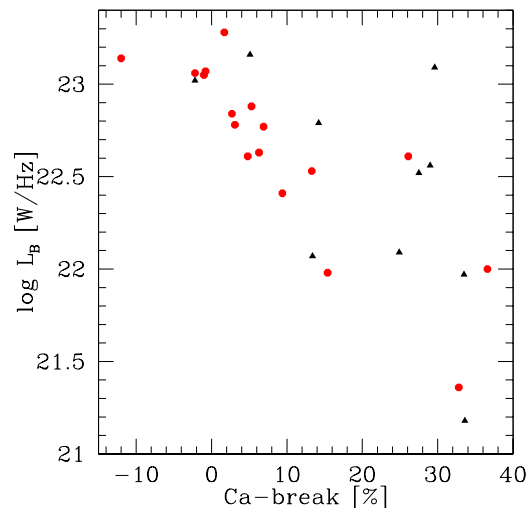


Fig. 2. Strength of the calcium break versus monochromatic luminosity L_B in the optical B-band. Circles refer to the *complete sample* while triangles mark additional objects found within the course of the work.

Ledden and O’Dell (1985) defined the overall spectral index between two frequencies:

$$\alpha_{1/2} = -\frac{\log(f_1/f_2)}{\log(\nu_1/\nu_2)} \quad (2)$$

Here f_1 and f_2 are the fluxes at two frequencies ν_1 and ν_2 . As reference frequencies we used 1.4 GHz in the radio ($\lambda \simeq 21 \text{ cm}$), 4400 \AA in the optical ($\sim B$), and 1 keV ($\lambda \simeq 12.4 \text{ \AA}$) in the X-ray region to derive the optical-X-ray α_{OX} , the radio-X-ray α_{RX} , and the radio-optical α_{RO} spectral index.

To compare these indices with those from the literature, shifts due to the use of different reference energies have to be taken into account. It can be shown that these shifts are small as long as the spectral shape within each band can be approximated by a single power law and the spectrum is not curved. Because the radio spectra are flat ($\alpha_R = 0$), the flux does not change when different reference frequencies are chosen in the radio domain. But by increasing the radio reference frequency, the α_{RX} and α_{RO} indices steepen. For example, if the reference frequency is changed from 1.4 to 5 GHz the radio-X-ray index changes by 6%: $\alpha_{RX}(5 \text{ GHz}, 1 \text{ keV}) \simeq 1.06 \times \alpha_{RX}(1.4 \text{ GHz}, 1 \text{ keV})$. If our spectral indices are compared with those using a larger X-ray reference energy, similar values for α_{OX} and α_{RX} are expected. Because of $f_\nu \propto \nu^{-\alpha}$, the expected flux at a higher energy is lower and the flux ratios increase. At the same time however, the frequency interval increases by about the same factor, if we assume $\alpha_E = 1$, which is a good approximation for the mean X-ray spectral energy index of BL Lac objects. The same reasoning applies for the optical region, where $\alpha_E \lesssim 1$, and larger changes of the relevant indices are not expected.

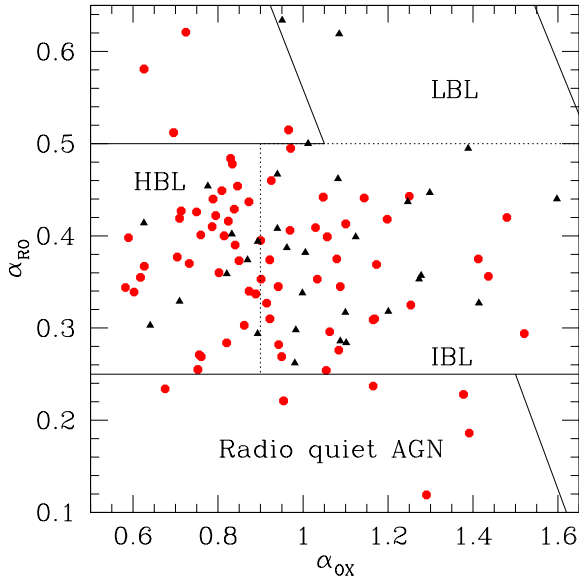


Fig. 3. The $\alpha_{OX} - \alpha_{RO}$ plane covered by the HRX-BL Lac objects. The points refer to the *complete sample*, the triangles mark additional objects found within the course of the work. Objects with $\alpha_{RO} < 0.2$ are called radio quiet.

The HRX-BL Lac sample shows typical values for the mean overall spectral indices: $\langle \alpha_{OX} \rangle = 0.94 \pm 0.23$, $\langle \alpha_{RX} \rangle = 0.55 \pm 0.08$, $\langle \alpha_{RO} \rangle = 0.37 \pm 0.09$, if compared to Wolter et al. (1998), Laurent-Muehleisen et al. (1999), and Beckmann et al. (2002).

The region in the $\alpha_{OX} - \alpha_{RO}$ plane, which is covered by the HRX-BL Lac sample, is shown in Figure 3. The center of the area covered by this sample is similar to that of the EMSS BL Lacs (see Padovani & Giommi 1995) though a larger range in α_{OX} and α_{RO} is covered.

4.1. Peak frequency

In order to get a more physical description of the spectral energy distribution of the BL Lac objects, we used a simple model to fit the synchrotron branch of the BL Lac. This has the advantage of describing the SED with one parameter (the peak frequency) instead of a set of three parameters (α_{OX} , α_{RO} , and α_{RX}). It has been shown by several authors that the synchrotron branch of the BL Lac SED is well approximated by a parabolic fit in the $\log \nu - \log \nu f_\nu$ plane (cf. Landau et al. 1986, Comastri et al. 1995, Sambruna et al. 1996, Fossati et al. 1998). In this way the peak position (ν_{peak}), the total luminosity and the total flux of the synchrotron emission can be derived. We chose the parameterization using fluxes $\log \nu f_\nu = a \cdot (\log \nu)^2 + b \cdot \log \nu + c$. Using luminosities instead of fluxes would change the absolute constant c only, leaving the position of the peak frequency unaffected.

If only three data points were given (one in the radio, optical, and X-ray band), the parabola was definite. When more than three data points were available (i.e. the K , H ,

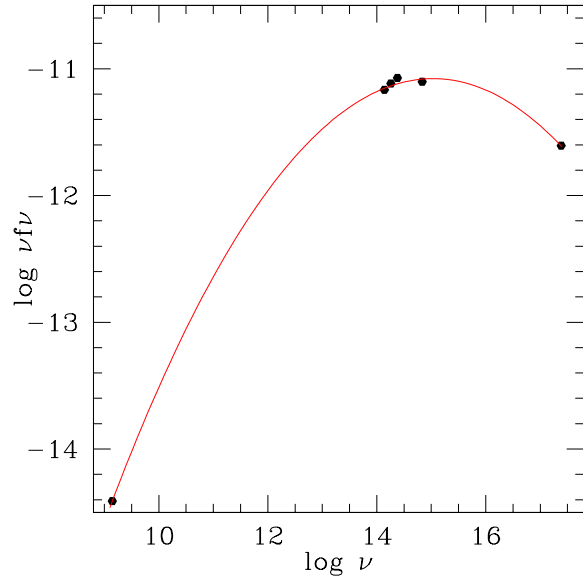


Fig. 4. Parabolic fit to the data of B2 0912+29.

and J near infrared measurements from the 2MASS), a χ^2 minimization was used to determine best fit parameters. In principle, also the spectral slope in the X-ray band could be used to constrain the fit further. Because of the large uncertainties involved deriving these slopes from hardness ratio in the RASS, they were used mostly for consistency checks. Only in cases, where the parabolic fit resulted in peak frequencies above the highest energies observed, i.e. for objects with $\log \nu_{\text{peak}}$ above 2 keV and steep X-ray spectra, the slopes were taken to account. An example for a parabolic fit is shown in Figure 4. ν_{peak} is sensitive for the f_x/f_{opt} -relation, and is therefore strongly correlated with α_{OX} . This is shown in Figure 5. The relation can be approximated by a polynomial of third degree. Using an F-test, parabolic fits of higher degree gave no improvements. Thus the peak frequency can also be determined, in the case no radio data is available by applying

$$\log \nu_{\text{peak}} = -3.0 \cdot \alpha_{OX}^3 + 13.8 \cdot \alpha_{OX}^2 - 23.3 \cdot \alpha_{OX} + 28.5 (\pm 0.51) \quad (3)$$

The standard error ($\sigma = 0.51$) is based on the deviation of the data points from the fit in Figure 5. This result is comparable to that found by Fossati et al. (1998) when studying the dependency of α_{RO} and α_{RX} on the peak frequency.

4.2. Correlation of luminosities with the SED

A set of physical parameters which are correlated to the peak frequency are the luminosities in the different wavelength regions. To compute luminosities for all objects, the unknown redshifts were set to $z = 0.3$ which is the mean value for the HRX-BL Lac sample. While the luminosities L_R in the radio, L_K in the near infrared, and L_B in the optical region are decreasing with increasing peak

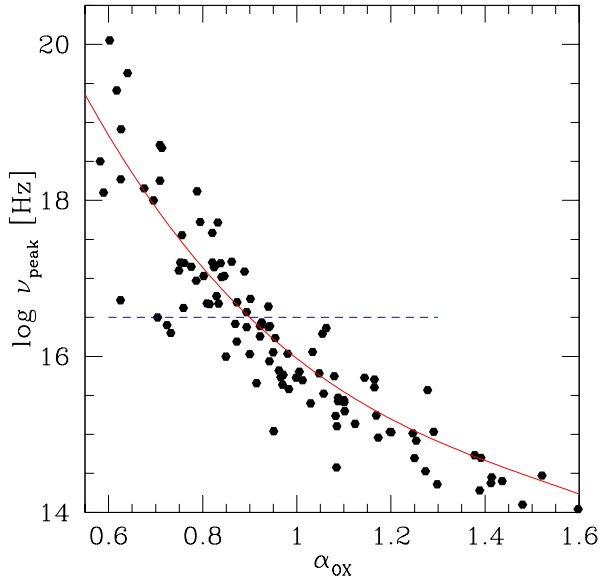


Fig. 5. Logarithm of the peak frequency vs. α_{OX} . The relation was approximated by a polynomial of third degree. The horizontal line marks the distinction between HBLs (above the line) and IBLs used in this paper.

frequency, the situation at X-ray energies is the other way round (as reported also by e.g. Mei, Zhang, & Jiang 2002, Beckmann 1999a).

The details about the correlation analysis are listed in Table 5, including the confidence level of the correlations.

The total luminosity L_{sync} within the synchrotron branch has been derived by integrating the spectral energy distribution between the radio and the X-ray band. This is a reasonable approximation as long as the peak frequency is below 1 keV ($\log \nu = 17.4$), but systematically underestimates L_{sync} if the peak frequency is shifted beyond 1 keV. The relation of peak frequency with the total luminosities does not show a clear correlation.

5. Distribution in space

5.1. V_e/V_a -test

Redshifts are available for 64 (83%) of the 77 BL Lac objects which form the *complete sample*. Therefore it is possible to determine a luminosity function for the HRX-BL Lacs and to study the evolution by application of an V_e/V_a -test. The direct images of the BL Lacs without redshift determination show point-like structure, and most of them have optical spectra consistent with high redshifts ($z > 0.5$). The difficulty in determining redshifts for them indicate that these objects are highly core dominated with the host galaxy outshined by the BL Lac core. This implies that the optical luminosity of these objects should be quite high.

The V_e/V_a -test is a simple method developed by Avni & Bahcall (1980) based on the V/V_{max} test of Schmidt

(1968). V_e stands for the volume, which is enclosed by the object, and V_a is the accessible volume, in which the object could have been found (e.g. due to a flux limit of a survey). Avni & Bahcall showed that different survey areas with different flux limits in various energy bands can be combined by the V_e/V_a -test. In the case of no evolution $\langle V_e/V_a \rangle = 0.5$ is expected and following Avni & Bahcall (1980) the error $\sigma_m(n)$ for a given mean value $\langle m \rangle = \langle V_e/V_a \rangle$ based on n objects is:

$$\sigma_m(n) = \sqrt{\frac{1/3 - \langle m \rangle + \langle m \rangle^2}{n}} \quad (4)$$

We computed the accessible volume $V_{a,i}$ for each object by applying the survey limits. In most cases this volume is determined by the X-ray flux limit, only $\sim 10\%$ of the objects have a smaller $V_{a,i}$ for the radio data, due to the radio flux limit of 2.5 mJy.

Applied to the *complete sample* the test yields $\langle V_e/V_a \rangle = 0.42 \pm 0.04$. This result shows that HBLs have been less numerous and/or less luminous in the past, but the significance is only 2σ . The negative evolution of X-ray selected BL Lac objects has been reported several times before. We also performed a K-S test in order to determine the probability of uniform V_e/V_a distribution, which would mean no evolution. For the whole HRX-BL Lac sample the probability of no evolution is rather small (3.5%).

Thanks to the large number of objects with known redshifts within the HRX-BL Lac sample it is possible to examine dependencies of the evolution on other parameters, like the overall spectral indices. A division into two groups (more and less X-ray dominated objects) according to α_{OX} was already made by Bade et al. (1998) for the *core sample* and resulted in a lower $\langle V_e/V_a \rangle = 0.34 \pm 0.06$ for the HBLs ($\alpha_{\text{OX}} < 0.9$) than for the IBLs within the sample. The $\langle V_e/V_a \rangle = 0.48 \pm 0.08$ for IBLs was even consistent with no evolution. Dividing the HRX-BL Lac sample accordingly we now get for the HBLs ($\alpha_{\text{OX}} < 0.9$) $\langle V_e/V_a \rangle = 0.45 \pm 0.05$ ($N=34$) and for the IBLs $\langle V_e/V_a \rangle = 0.40 \pm 0.06$ ($N=30$). The difference between the two groups has practically vanished, and we are thus not able to confirm the different types of evolution for the HBLs and the IBLs. But still there are 13 objects within the HRX-BL Lac sample without known redshift, and nearly all of them are IBLs. Including them into the V_e/V_a -test by assigning them either the mean redshift of our sample ($z = 0.3$) or a high redshift ($z = 0.7$) does not change the mean V_e/V_a values significantly. The results of the different V_e/V_a -tests are shown in Table 6. Assigning even higher redshifts would increase the V_e/V_a for the IBLs, but we consider this unlikely, as the luminosities would then become exceptionally high. For example in 0716+714, PG 1246+586, or PG 1437+398 the X-ray luminosities would exceed values of $L_X = 10^{46}$ erg s $^{-1}$ in the 0.5 – 2.0 keV range.

We conclude therefore that the HRX sample shows no difference in evolution for HBLs and IBLs. The results presented here are in good agreement with recent other investigations on the evolutionary behaviour of BL

Table 5. Correlation of luminosity with peak frequency in the extended HRX-BL Lac sample

region	r_{xy} Pearson coefficient	confidence level of correlation	linear regression ^a
radio (1.4 GHz)	-0.23	> 97%	$\log L_R = -0.09 \cdot \log \nu_{\text{peak}} + 26.4$
near IR (K-band)	-0.28	> 95% ^b	$\log L_K = -0.14 \cdot \log \nu_{\text{peak}} + 25.9$
optical (B-band)	-0.37	> 99.9%	$\log L_B = -0.13 \cdot \log \nu_{\text{peak}} + 25.1$
X-ray (1 keV)	+0.51	> 99.9%	$\log L_X = +0.19 \cdot \log \nu_{\text{peak}} + 17.3$
total (radio – X-ray)	-0.12		$\log L_{\text{sync}} = -0.04 \cdot \log \nu_{\text{peak}} + 22.0$

^a Luminosities in [W/Hz]^b The lower confidence level results from the lower number of objects (52) with known K-band magnitudes. The other correlations are using the 104 BL Lacs of the extended sample.**Table 6.** Results from the V_e/V_a -tests for the HRX-BL Lac *complete sample*

selection	unknown z set to	N^a	$\langle V_e/V_a \rangle$	K-S ^b [%]
all (known z)	-	64	0.42 ± 0.04	3.5
all	0.3	77	0.44 ± 0.03	5.3
all	0.7	77	0.46 ± 0.03	5.3
HBLs (known z)	-	34	0.45 ± 0.05	24.0
all HBLs	0.3	36	0.48 ± 0.05	46.1
all HBLs	0.7	36	0.48 ± 0.05	46.1
IBLs (known z)	-	30	0.40 ± 0.06	14.0
all IBLs	0.3	41	0.41 ± 0.05	10.7
all IBLs	0.7	41	0.43 ± 0.05	10.7

^a number of objects used for this test^b K-S test probability that the V_e/V_a values have a uniform distribution in the [0...1] interval (probability for no evolution).**Table 7.** Results from the V_e/V_a -tests for comparable investigations

survey	selection	unknown z	N^a	$\langle V_e/V_a \rangle$
REX	total	0.27	55	0.48 ± 0.04
REX	HBL	0.27	22	0.49 ± 0.06
sedentary	total	0.25	155	0.42 ± 0.02
DXRBS	all BL Lacs	0.40	30	0.57 ± 0.05
DXRBS	HBL	0.40	11	0.65 ± 0.09
DXRBS	LBL	0.40	19	0.52 ± 0.07

^a number of objects used for this test

Lac objects, as shown in Table 6. Except the sedentary survey (Giommi, Menna, & Padovani 1999) none of the studies could confirm the highly significant negative evolution found e.g. by Bade et al. (1998 for the HRX-BL Lac *core sample* or by Wolter et al. (1994) for the EMSS BL Lacs. The best sample to be compared with should be the REX survey, which also uses the combination of RASS and NVSS data, although going to lower X-ray flux limits while using only the are of the PSPC pointed observation. The REX has also a mean redshift of $z = 0.3$

and the $\langle V_e/V_a \rangle$ are within one sigma when compared to the HRX-BL Lac sample.

5.2. X-ray Luminosity functions

For the V_e/V_a -test the knowledge of the redshifts is of minor importance. However, the luminosity function which defines the space density at a given object luminosity can only be derived when having a complete sample with known distances. Based on this function we wish to estimate the fraction of AGN which appear to be BL Lac objects. To determine the cumulative luminosity function (CLF), one has to count all objects within a *complete sample* above a given luminosity, and divide this number by the volume V_a which has been surveyed for these objects. We follow here the procedure described by Marshall (1985) to derive the space density and the corresponding errors. The survey area of the HRX-BL Lac *complete sample* is 4768 deg^2 (Table 1). Because the fraction of objects without known redshift is 17% the effective area which is used to compute the luminosity function is decreased by this fraction to 3959 deg^2 . This implies that the redshift distribution of the missing objects is the same as for the rest. As discussed before, this assumption might be incorrect, as we expect many of them having rather high redshifts. The effect of different evolution for high and low redshift objects, described in the next paragraph, would be even stronger in this case.

The *complete sample* is large enough to divide it into a high redshift and a low redshift bin in order to examine possible differences in their CLF. The dividing value was set to the median of the HRX-BL Lac sample $z_{\text{median}} = 0.272$. To derive high and low redshift CLFs the accessible volume $V_{a,i}$ for the objects with $z < 0.272$ has been restricted to $z = 0.272$ whenever $z_{\text{max},i} > 0.272$. For the high redshift objects the accessible volume was computed from $z = 0.272$ up to $z_{\text{max},i}$. The resulting two cumulative luminosity functions are shown in Figure 6.

There seem to be differences between the high and low redshift CLF. The slope of the low redshift CLF is flatter. A linear regression gives a slope of -0.9 while for $z > 0.272$ the slope is -1.4 . But in the overlapping regime at $L_X(0.5 - 2.0 \text{ keV}) \sim 10^{45}$ the luminosity functions show similar slopes.

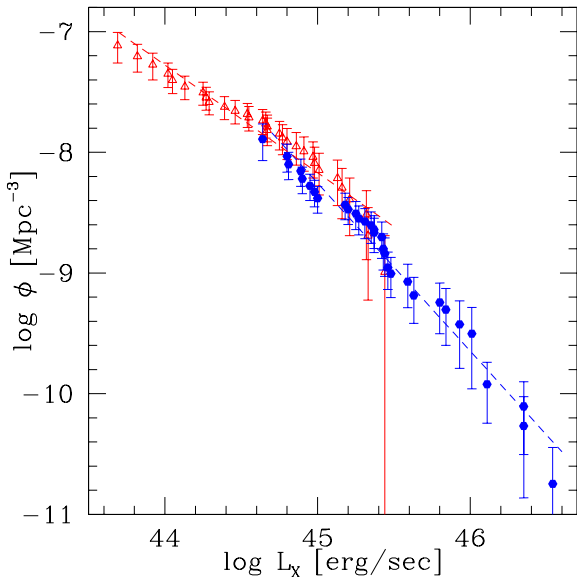


Fig. 6. Cumulative luminosity function of the two subsamples with $z > 0.272$ (circles) and $z < 0.272$ (open triangles).

The left panel of Figure 7 shows the comparison of the HRX-BL Lac *complete sample* X-ray luminosity function with the results from the EMSS BL Lac sample (Wolter et al. 1994, Padovani & Giommi 1995). The expected luminosities of the HRX-BL Lacs within the EINSTEIN IPC energy band (0.3 – 3.5 keV) were calculated assuming a spectral slope of $\alpha_X = 1.0$. Space densities are given as number of objects per Gpc^3 and X-ray luminosity bin following Padovani & Giommi (1995). The data from the EMSS are consistent with those from the HRX-BL Lac *complete sample* within the 1σ error bars. The marginal differences can be due to systematic errors for the calculated luminosities in the IPC band because of differing spectral slopes, or resulting from differences in the calibration of the IPC and the PSPC detectors.

In the right panel of Figure 7 we compare the differential luminosity function of the *complete sample* with the corresponding function for AGNs at $z < 0.5$. The AGN X-ray luminosity function was taken from the ROSAC sample (“A ROSAT based Search for AGN-Clusters”, Tesch 2000). This AGN sample was constructed similarly as the HRX-BL Lac sample and both samples match closely in brightnesses and redshifts. The ROSAC-AGN sample contains 182 RASS-AGNs with $z < 0.5$ identified in an area of 363 deg^2 in the constellation of Ursa Major. The AGN X-ray luminosities have been corrected for the different X-ray band (0.1 – 2.4 keV instead 0.5 – 2.0 keV) using the same spectral slopes used for the ROSAC sample.

We find that the space density of BL Lacs in the luminosity range $44 < \log L_X < 46$ is about 10% of the space density of AGNs. In case that all AGNs have jets and would be classified as BL Lacs when looking into their jet, an jet opening angle of $\sim 50^\circ$ would follow. But as

the jet emission is expected to be beamed, the BL Lacs appear to be brighter than they are. Following Urry & Shaefer (1984) the observed luminosity is $L_{obs} = \delta^p L_{emi}$ with L_{emi} being the emitted luminosity, and

$$\delta = \frac{1}{\gamma(1 - \frac{v}{c_0} \cos \theta)} \quad (5)$$

where γ is the Lorentz factor of the jet emission. p depends on the spectral slope and the jet flow model. For the simple case of a moving blob and continuous reacceleration (Lind & Blandford 1985) which applies e.g. for the model of a wide X-ray jet (Celotti et al. 1993) the exponent is $p = 3 + \alpha$, where $\alpha \simeq 1$ is the spectral index. For a conical jet this exponent is $p = 2 + \alpha$ (Urry & Shaefer 1984). Assuming an jet opening angle of $\theta \sim 30^\circ$ (Urry & Padovani 1995) and a Lorentz factor $\gamma \sim 5$ the amplification factor is $\delta^p \simeq 50$ (for the conical jet) and $\delta^p \simeq 200$ (for the wide X-ray jet). Correcting the luminosities accordingly yields a fraction of $\leq 0.1\%$ BL Lacs among all AGNs. A smaller opening angle and/or larger Lorentz factor would lead to an even lower BL Lac fraction among the AGN.

6. Discussion

The large number of objects included in the HRX-BL Lac sample enabled us to study in detail a number of BL Lac properties in different wavelength regions. In the following, we will discuss these properties with special emphasis on their compatibility with the most recent models trying to unify the HBL and LBL objects.

6.1. Strength of the calcium break and luminosities

We observed a clear anti-correlation between calcium break strength and the luminosity in the radio, near infrared, optical, and X-rays bands. We explain this with a wide range of luminosities for the non-thermal source, while the host galaxies seem to have approximately constant luminosity. The higher the luminosity of the central source, the more does the core outshine the hosting galaxy, leading to decreasing break strength with increasing luminosity.

The identification of several HRX-BL Lac with $25\% < \text{Ca} - \text{break} < 40\%$ and the smooth extension of the correlation between break strength and luminosities into this range, supports previous findings that BL Lacs can have $\text{Ca} - \text{break} > 25\%$ (Marchã et al. 1996; Laurent-Muehleisen et al. 1999; Rector et al. 2000; Landt et al. 2002) in contrast to earlier suggestions (Stocke et al. 1989).

Landt et al. (2002) studied in detail the dependency of the Calcium break strength on the luminosity of the blazars inside the DXRBS sample (Padovani 2001). They found the same correlation as described here for the HRX-BL Lac sample and show that the Calcium break values decrease with increasing jet power, and therefore with increasing luminosity. Based on this they conclude that the break value of BL Lac objects could be an indicator of

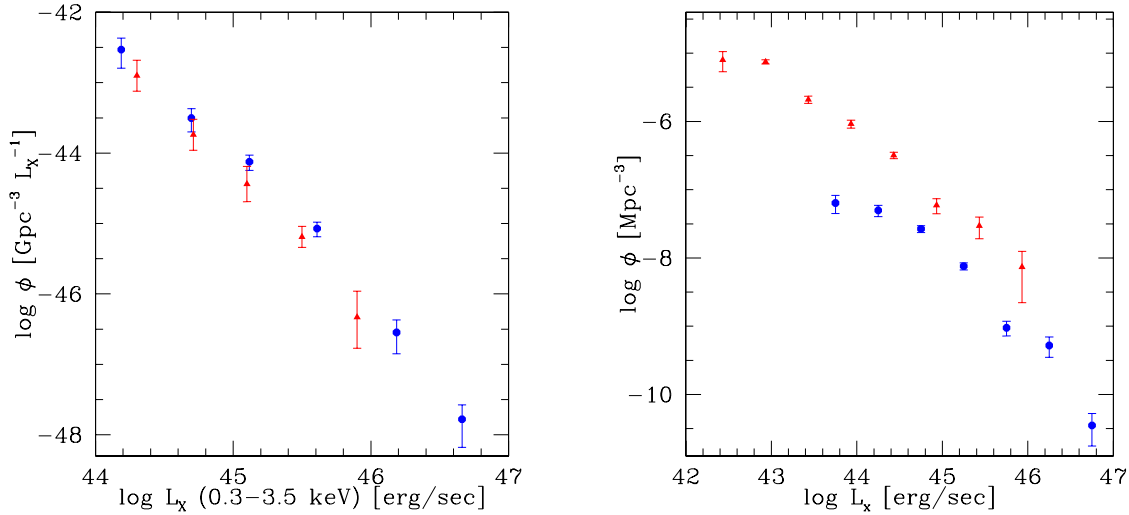


Fig. 7. Left panel: The differential X-ray luminosity function of the HRX-BL Lac *complete sample* (circles) in comparison to EMSS BL Lacs (triangles; Padovani & Giommi 1995). The X-ray data of the HRX-BL Lac objects have been extrapolated to the EINSTEIN IPC energy band assuming a spectral slope of $\alpha_X = 1$. Right panel: Comparison of the X-ray luminosity function of RASS selected AGNs from the ROSAC sample (triangles; Tesch 2000) with HRX-BL Lacs (circles). The density of BL Lacs is ~ 10 times lower than for all AGNs.

the orientation. Nevertheless different luminosities of the core component (i.e. of the jet) will also play a major role in the effect, and it seems to be difficult to disentangle the influence from different orientation and from different jet luminosity. Thus though we find for the HRX-BL Lac sample the same correlation as described by Landt et al. 2002 we conclude here only that the break strength is an indicator of different apparent luminosity, either based on different orientation, or on different jet power, or on mixture of both effects.

6.2. HBL/LBL: evolutionary dichotomy?

Most of the results for the HRX-BL Lac *core sample* (Bade et al. 1998) could be confirmed by the *complete sample* presented here. The most significant discrepancy are the different results of the V_e/V_a test. We found negative evolution using the *complete sample*, but we did not find differences in evolution, if we divide the sample by α_{OX} (or peak frequency).

The results of Bade et al. (1998) could have been arisen from selection effects due to the “patchy” search area used. A Monte-Carlo simulation done on the HRX-BL Lac *complete sample* shows however, that this is not the case. By randomly selecting a subsample of 17 BL Lac objects (which is the number of objects for which Bade et al. found different types of evolution) out of the HBLs of the *complete sample* there is a chance of $< 1\%$ only to find a $\langle V_e/V_a \rangle < 0.35$.

Another reason for the different results could be related to the different treatment of the radio properties. As radio detection was not a selection criterium in Bade et al., no radio flux limit was taken into account. Applying here the V_e/V_a -test to the *complete sample* (cf. Sect. 5), the ac-

cessible volume V_a was determined for $\approx 10\%$ of the objects by the radio limit. The V_e/V_a values are correspondingly increased compared to the case where only X-ray flux limit is taken into account, resulting in a less negative evolution. There remains the fact that no BL Lac objects were found yet, with $f_R < 2$ mJy radio counterparts and the question is still open whether this is a selection effect or not. It could be that our decision to apply the radio detection as selection criterium weakens the negative evolution found in pure X-ray selected samples.

The result, that the evolution of BL Lac objects of the HBL and IBL type is consistent with no evolution is in good agreement with other recent studies. Neither REX or DXRBS, nor the HRX-BL Lac sample show a difference for the more or less X-ray dominated BL Lacs. On the contrary it seems that the evolution of the IBL might even be slightly more positive than that of the HBL class. This picture clearly differs from the EMSS BL Lac result of $\langle V_e/V_a \rangle = 0.36 \pm 0.05$, while the serendipitous survey, presented by Giommi, Menna & Padovani 1999 seems not be complete enough up to now to draw a firm conclusion. Caccianiga et al. (2002) argue, that the REX might miss the negative evolution of the HBL is not visible simply because the sample is not deep enough, and this argumentation then would also apply for the HRX-BL Lac sample, which X-ray flux limit is about two times higher than that of the REX BL Lacs. Their simulation result in the conclusion that even a completion of the REX survey might not lead to a highly significant negative evolution (2σ for the simulated sample).

Finally, the evolution found in the course of this work is in good agreement with that of FR-I galaxies ($\langle V_e/V_a \rangle = 0.40 \pm 0.06$) within the 3CR sample (Laing et al. 1984). This supports the assumption that the FR-I galaxies build

the parent population of BL Lac objects (see e.g. Padovani & Urry 1990).

In contrast to HBLs, the LBLs show weak or positive evolution ($\langle V_e/V_a \rangle = 0.61 \pm 0.05$) as shown for the 1Jy sample by Rector & Stocke (2001). Following the sequence of blazars, also FSRQs exhibit significant positive evolution ($\langle V_e/V_a \rangle = 0.58 \pm 0.03$ for the 119 FSRQs in the DXRBS sample; Padovani 2001). Also FR-II radio galaxies and “normal” quasars seem to be more numerous and/or luminous at cosmological distances than in the neighborhood, leaving the question for the reasons of the HBL/LBL evolutionary dichotomy of relevance also in future.

6.3. A unifying model for LBL and HBL

The different evolutionary behaviour of HBLs and LBLs is a challenge for all theories to unify both BL Lac types into one class. However, the existence of transition objects and the numerous similar properties of LBLs and HBLs make it plausible that both classes belong to the same parent population.

As described by Böttcher & Dermer (2002) one way to unify both classes would be a transformation of LBLs into HBLs as the BL Lac objects grow older. In this model, BL Lac objects start as LBLs with jets of high energy densities. Strong cooling limits the electron energies leading to cutoff frequencies for the synchrotron component at optical wavelengths and for the IC component in the GeV energy range. As shown by Beckmann et al. (2002), this results in steep X-ray spectra with strong curvature. The core outshines the host galaxy leading to a low calcium break value (Landt et al. 2002) as seen also for the HRX-BL Lac sample (cf. Fig. 2).

When by the time the source of the jet gets less powerful the energy density within the jet decreases (Tavecchio et al. 1998). The cooling efficiency decreases as well resulting in higher cutoff frequencies for HBLs. The shift of the cutoff frequencies to higher energies is therefore accompanied by decreasing bolometric luminosities, which is evident from the decrease of the luminosities in the radio, near IR and optical bands. Due to the increasing peak frequencies of the synchrotron branch more energy is released in the X-ray band and the X-ray luminosity increases quite in contrast to the luminosities at shorter frequencies (cf. Table 5). The X-ray spectra are correspondingly flatter and less curved than in the LBL state (Beckmann & Wolter 2001).

Objects which do not fit into this scenario are doubtlessly the extremely luminous HBLs, like 1ES 1517+656 (Beckmann et al. 1999b). The scenario presented here assumes the HBLs to be on average less luminous than the LBLs. Apart from the exceptionally high X-ray luminosity, this object also shows an optical luminosity typical for a Flat Spectrum Radio Quasar (FSRQ). Padovani 2001 argues that those high state BL Lacs with high peak frequency might belong to the high energy peaked FSRQ class (HFSRQ), flat-spectrum radio quasars

with synchrotron peak in the UV/X-ray band. In this case 1ES 1517+656 should show strong emission lines, e.g. H_α and H_β which would be located in the near infrared for this high-redshift BL Lac ($z = 0.7$) and would have been missed by previous observations.

The HRX-BL Lac sample could be the basis to study the extreme end of the HBL population, the ultra high frequency peaked BL Lac objects (UHBL). Sambruna et al. (1996) argued that objects with cutoff frequencies higher than 10^{18} Hz would be detected only in hard X-ray surveys but should be faint at lower frequencies, which would make their discovery difficult.

Nevertheless HBLs have already been detected at TeV energies, as e.g. 1ES 1426+428 (Aharonian et al. 2002; Horan et al. 2002) and 1ES1959+650 (Horns & Konopelko 2002). Recently Costamante & Ghisellini (2002) showed that it is possible to select candidates for TeV BL Lacs on the basis of the knowledge of the SED, i.e. strong X-ray flux and a sufficiently strong radio-through-optical flux, which results in high peak frequencies of the synchrotron branch.

Also 13 HBLs within the HRX-BL Lac sample show peak frequencies $\nu_{peak} > 10^{18}$ Hz from the parabolic fit to the synchrotron branch and three objects even $\nu_{peak} > 10^{19}$ Hz. 1RXS J121158.1+224236 might even be a UHBL with a peak frequency of the synchrotron branch at $\nu_{peak} \simeq 10^{22}$ Hz. To confirm the high peak frequencies, for this extreme source, observations with the BeppoSAX satellite have been performed and results will be presented in a forthcoming paper. Investigations in the gamma region (~ 1 MeV) are needed to decide whether these energies are dominated by the synchrotron emission or if already the inverse Compton branch is rising. The SPI spectrograph on-board the INTEGRAL mission (see e.g. Winkler & Hermsen 2000), which has been successfully launched in October 2002, will allow to do spectroscopy in this energy region (20 keV – 8 MeV).

Acknowledgements. We would like to thank the anonymous referee for the valuable suggestions which helped us to improve the paper. This research has made use of the NASA/IPAC Extragalactic Database (NED) which is operated by the Jet Propulsion Laboratory, California Institute of Technology under contract with the National Aeronautics and Space Administration. We acknowledge support by the Deutsche Forschungsgemeinschaft through grants Re 353/39-1 and En 176/23-1.

References

- Aharonian, F., Akhperjanian, A., Barrio, J., et al. 2002, *A&A* 384, L23
- Avni, Y., & Bahcall, J. N. 1980, *ApJ* 235, 694
- Bade, N., Beckmann, V., Douglas, N. G., et al. 1998, *A&A* 334, 459
- Beckmann, V. 1999a, in: *PASPC Vol. 159*, eds. L. O. Takalo, A. Silanpää
- Beckmann, V., Bade, N., & Wucknitz, O. 1999b, *A&A* 352, 395
- Beckmann, V. 2000a, *BLAZAR Data* 2, 3

- Beckmann, V. 2000b, PhD thesis, Hamburg University, <http://www.sub.uni-hamburg.de/disse/330/vbdiss.html>
- Beckmann, V., & Wolter, A. 2001, AIP conference proceedings 599, 502, astro-ph/0007089
- Beckmann, V., Wolter, A., Celotti, A., et al. 2002, A&A 383, 410
- Bicknell, G. V., & Wagner, S. J. 2002, PASA 19, 129
- Böttcher, M., & Dermer, C. D. 2002, ApJ 564, 86
- Böttcher, M., & Chiang, J. 2002, ApJ 581, 127
- Caccianiga, A., Maccacaro, M., Wolter, A., et al. 1999, ApJ 513, 51
- Caccianiga, A., Maccacaro, M., Wolter, A., et al. 2002, ApJ 566, 181
- Cavaliere, A., & D'Elia, V. 2002, ApJ 571, 226
- Celotti, A., Maraschi, L., Ghisellini, G., et al. 1993, ApJ 416, 118
- Comastri, A., Molendi, S., & Ghisellini, G. 1995, MNRAS 277, 297
- Condon, J.J., Cotton, W. D., Greisen, E. W., et al. 1998, AJ 115, 1693
- Costamante, L., & Ghisellini, G. 2002, A&A 384, 56
- Dressler, A., & Shectman, S. 1987, AJ 94, 899
- Fossati, G., Maraschi, L., Celotti, A., et al. 1998, MNRAS 299, 433
- Georganopoulos, M., Marscher, A. P. 1998, ApJ 506, 621
- Ghisellini, G., Padovani, P., Celotti, A., & Maraschi, L. 1993, ApJ 407, 65
- Ghisellini, G., Celotti, A., Fossati, G., et al. 1998, MNRAS 301, 451
- Giommi, P., Menna, M. T., Padovani, P. 1999, MNRAS 310, 465
- Ghisellini, G., Celotti, A., Costamante L. 2002, A&A 386, 833
- Hagen, H.-J., Groote, D., Engels, D., & Reimers, D. 1995, A&AS 111, 195
- Horan, D., Badran, H. M., Bond, I. H., et al. 2002, ApJ 571, 753
- Horns, D., & Konopelko, K. 2002, ATel 96, 1
- Landau, R., Golisch, B., Jones, T. J., et al. 1986, ApJ 308, 78
- Landt, H., Padovani, P., Perlman, E. S., et al. 2001, MNRAS 323, 757
- Landt, H., Padovani, P., & Giommi, P. 2002, MNRAS 336, 945
- Laurent-Muehleisen, S. A., Kollgaard, R. I., Feigelson I. D., et al. 1999, ApJ 525, 127
- Ledden, J. E., & O'Dell, S. L. 1985, ApJ 298, 630
- Lind, K.R., & Blandford, R. D. 1985, ApJ 295, 358
- Maccacaro, M., Caccianiga, A., Della Ceca, R., et al. 1998, Astron. Nachr. 319, 15
- Madau, P., Ghisellini, G., & Persic, M. 1987, MNRAS 224, 257
- Maraschi, L., & Rovetti, F. 1994, ApJ 436, 79
- Maraschi, L., & Tavecchio, F. 2002, ApJ in press, astro-ph/0205252
- Marchã, M. J. M., Browne, I. W. A., Impey, C. D., & Smith, P. S. 1996, MNRAS 281, 425
- Marshall, H. L. 1985, AJ 299, 109
- Mei, D. C., Zhang, L., & Jiang, Z. J. 2002, A&A 391, 917
- Padovani, P., & Urry, C. M. 1990, ApJ 356, 75
- Padovani, P. 1992, MNRAS 257, 404
- Padovani, P., & Giommi, P. 1995, ApJ 444, 567
- Padovani, P. 2001, Blazar Demographics and Physics, ASP Conf Series, 227, 163
- Padovani, P., & Urry C. M. 2001, Blazar Demographics and Physics, ASP Conf Series, 227
- Perlman, E. S., Padovani, P., Giommi, P., et al. 1998, AJ 115, 1253
- Rector, T. A., Stocke, J. T., Perlman, E. S., et al. 2000, AJ 120, 1626
- Rector, T. A., & Stocke, J. T. 2001, AJ 122, 565
- Sambruna, R. M., Maraschi, L., & Urry, C. M. 1996, ApJ 463, 444
- Schartel, N. 1994, PhD thesis, MPE Garching
- Schmidt, M. 1968, ApJ 151, 393
- Skrutskie, M. F., Beichmann, C., & Capps, R. 1995, American Astronomical Society Meeting 187, 75.07
- Stiening, R., Skrutskie, M. F., & Capps, R. 1995, American Astronomical Society Meeting 187, 75.08
- Stickel, M., Fried, J. W., & Kühr, H. 1991, ApJ 374, 431
- Stocke, J. T., Morris, S. L., Gioia, I. M., et al. 1989, in: BL Lac Objects, ed. L. Maraschi, T. Maccacaro, & M.-H. Ulrich (Berlin:Springer), 242
- Stocke, J. T., Morris, S. L., Gioia, I. M., et al. 1991, ApJS 76, 813
- Tavecchio, F., Maraschi, L., & Ghisellini, G. 1998, ApJ 509, 608
- Tesch, F., Carrera, F.J., Engels, D., et al. 2000, in: Large Scale Structure in the X-ray Universe, Proceedings of the 20-22 September 1999 Workshop, Santorini, Greece, eds. Plionis, M. & Georgantopoulos, I., Atlantisciences, Paris, France, p. 407
- Tesch, F. 2000, PhD thesis, Hamburg University, <http://www.sub.uni-hamburg.de/disse/284/Disse.pdf>
- Urry, C. M., & Shaefer, R. A. 1984 ApJ 280, 569
- Urry, C. M., & Padovani, P. 1995, PASP 107, 803
- Urry, C. M., Scarpa, R., O'Dowd, M., et al. 2000, ApJ 532, 816
- Voges, W., Aschenbach, B., Boller, Th., et al. 1999, A&AS 349, 389
- Wall, J. V., & Peacock, J. A. 1985, MNRAS 216, 173
- Winkler, C., & Hermsen, W. 2000, AIP Conference Proceedings, 510, 676
- Wolter, A., Caccianiga, A., Della Ceca, R., & Maccacaro, T. 1994, ApJ 433, 29
- Wolter, A., Comastri, A., Ghisellini, G., et al. 1998, A&A 335, 899

7. Appendix: Tables to the HRX-BL Lac sample

Table 8. Objects from the RASS-BSC/NVSS correlation. An X-ray count rate limit $hcps \geq 0.09$ was applied.

α	δ	Name	Redshift ^a	Classification ^a
07 04 27.0	63 18 56	KUG 0659+633	0.095	G
07 07 13.5	64 35 58	VII Zw 118	0.080	Sy1
07 09 07.6	48 36 57	NGC 2329	0.019	G S0-:
07 10 30.0	59 08 08	87GB 070609.2+591323	0.125	BL Lac
07 11 48.0	32 19 02	PGC 020369	0.067	Sy2
07 13 39.7	38 20 43	IRAS F07102+3825	0.123	NLSy1
07 18 00.7	44 05 27	IRAS F07144+4410	0.061	Sy1
07 21 53.2	71 20 31	0716+714		BL Lac
07 22 17.4	30 30 52	HS 0719+3036	0.100	Sy1.5
07 32 21.5	31 37 50	1RXS J073221.5+313750	0.170	G
07 36 24.8	39 26 08	FBS 0732+396	0.118	Sy1
07 40 58.5	55 25 33	CGCG 262-019	0.034	GGroup
07 41 44.8	74 14 45	ZwCl 0735.7+7421	0.216	GClstr
07 42 32.9	49 48 30	UGC 03973	0.022	Sy1.2
07 42 50.3	61 09 31	87GB 073825.7+611711		star (K0)
07 44 05.6	74 33 56	MS 0737.9+7441	0.315	BL Lac
07 45 41.2	31 42 50	[HB89] 0742+318	0.461	Sy1
07 47 29.4	60 56 01	UGC 04013	0.029	Sy1.2
07 49 06.2	45 10 40	B3 0745+453	0.190	Sy1
07 49 29.4	74 51 42	87GB[BWE91] 0743+7458	0.607*	BL Lac*
07 51 22.1	55 11 56	1RXS J075122.1+551156	0.302*	Sy1*
07 52 43.6	45 56 53	NPM1G +46.0092	0.060	Sy1.9
08 01 32.3	47 36 19	87GB 075755.8+474440	0.158	Sy1
08 01 47.8	56 33 16	NGC 2488	0.029	G, S0-:
08 05 25.8	75 34 24	WN B0759.1+7542	0.121	BL Lac
08 06 25.5	59 31 05	87GB 080212.8+593933		BL Lac
08 09 38.5	34 55 44	MG2 J080937+3455	0.082	BL Lac ^C
08 09 49.2	52 18 55	87GB 080601.8+522753	0.138	BL Lac
08 10 59.0	76 02 45	PG 0804+761	0.100	Sy1
08 15 17.8	46 04 29	KUG 0811+462	0.041	Sy1.5
08 19 26.6	63 37 41	KOS NP6 038	0.118 ^C	G, E ^C
08 19 29.5	70 42 21	1RXS J081929.5+704221	0.001	HolmbergII
08 22 09.5	47 06 01	RGB J0822+470	0.127	Sy1.5
08 32 25.1	37 07 37	FIRST J083225.3+370737	0.091	Sy1.2
08 32 51.9	33 00 11	1RXS J083251.9+330011	0.671	BL Lac
08 36 58.3	44 26 13	[HB89] 0833+446	0.255	QSO
08 38 11.0	24 53 36	NGC 2622	0.029	Sy1.8
08 41 25.1	70 53 43	[HB89] 0836+710	2.172	blazar
08 42 03.4	40 18 30	KUV 08388+4029	0.152	Sy1
08 42 55.9	29 27 52	ZwCl 0839.9+2937	0.194	GClstr
08 59 16.5	83 44 50	1RXS J085916.5+834450	0.327*	BL Lac*
08 59 30.1	74 55 10	1RXS J085930.1+745510	0.276	Sy1
09 09 53.9	31 05 58	MG2 J090953+3104	0.274*	BL Lac*
09 13 24.6	81 33 18	1RXS J091324.6+813318	0.639*	BL Lac*
09 15 52.2	29 33 35	B2 0912+29 / TON 0396		BL Lac ^C
09 16 51.8	52 38 29	87GB 091315.6+525108	0.190	BL Lac

The objects of the BSC/NVSS correlation

α	δ	Name	Redshift ^a	Classification ^a
09 23 43.0	22 54 37	CGCG 121-075	0.032	Sy1
09 25 12.3	52 17 17	MRK 0110	0.035	Sy1
09 27 02.8	39 02 21	[HB89] 0923+392	0.695	Sy1
09 28 04.2	74 47 14	87GB 092308.0+745942	0.638	BL Lac
09 30 37.1	49 50 28	1ES 0927+500	0.186	BL Lac
09 33 46.5	62 49 43	1RXS J093346.5+624943		star G5
09 35 27.4	26 17 14	1RXS J093527.4+261714	0.122	Sy1
09 47 13.2	76 23 17	RBS 0797	0.354	LINER
09 52 25.8	75 02 16	1RXS J095225.8+750216	0.178*	BL Lac*
09 55 34.7	69 03 38	MESSIER 081	-0.00011	LINER/Sy1.8
09 55 50.4	69 40 52	MESSIER 082	0.00068	Starburst G
09 59 29.8	21 23 40	87GB 095643.1+213755	0.365 ^C	BL Lac ^C
10 00 28.9	44 09 10	1RXS J100028.9+440910	0.154	GClstr
10 02 35.9	32 42 19	NGC 3099	0.051	G
10 05 42.2	43 32 44	IRAS 10026+4347	0.178 ^C	Sy1 ^C
10 06 39.1	25 54 51	PGC 029375	0.116	GClstr
10 08 11.5	47 05 26	1RXS J100811.5+470526	0.343	BL Lac ^C
10 09 16.7	71 10 40	87GB 100504.8+712548	0.193	GClstr
10 10 27.9	41 32 42	[HB89] 1007+417	0.612	QSO
10 12 44.4	42 29 59	B3 1009+427	0.376 ^C	BL Lac ^C
10 15 04.3	49 26 04	[HB89] 1011+496	0.200	BL Lac
10 16 16.4	41 08 17	FIRST J101616.8+410812	0.281	BL Lac
10 16 55.5	73 23 59	NGC 3147	0.009	Sy2
10 17 18.0	29 14 39	IRAS F10144+2929	0.048	Sy1
10 19 00.8	37 52 50	FIRST J101900.4+375240	0.133	Sy1
10 19 12.1	63 58 03	MRK 141	0.042	Sy1.5
10 22 12.5	51 24 06	MS 1019.0+5139	0.141	BL Lac
10 22 28.9	50 06 30	ABELL 0980:[CAE99]	0.158	G
10 30 58.8	31 03 06	[HB89] 1028+313	0.178	Sy1
10 31 05.7	82 33 27	1RXS J103105.7+823327		star F2V
10 31 18.6	50 53 41	1ES 1028+511	0.361	BL Lac ^C
10 32 14.3	40 16 07	[BBN91] 102920+403136	0.078	GClstr
10 34 23.1	73 45 25	NGC 3252	0.004	G, SBd?sp
10 34 38.7	39 38 34	KUG 1031+398	0.042	Sy1
10 34 59.5	30 41 39	Abel 1045	0.137	GClstr
10 38 46.7	53 30 02	SN 1991N	0.003	SNR in NGC3310
10 40 43.7	39 57 06	IRAS F10378+4012	0.139	Sy2
10 44 27.6	27 18 13	1RXS J104427.6+271813		G
10 44 39.4	38 45 42	CGCG 212-045	0.036	Sy1.5
10 45 20.5	45 34 04	1RXS J104520.5+453404		star B8V
10 51 25.1	39 43 29	FIRST J105125.3+394325	0.498*	BL Lac*
10 55 44.0	60 28 10	1RXS J105544.0+602810		var. K0 star
10 57 23.5	23 03 17	1RXS J105723.5+230317	0.378 ^C	BL Lac ^C
10 58 25.9	56 47 16	RX J1058+5647		prob. GClstr*
10 58 37.5	56 28 16	87GB 105536.5+564424	0.144	BL Lac
11 00 21.3	40 19 33	FIRST J110021.0+401927	0.225*	BL Lac ^C
11 04 12.4	76 58 59	PG 1100+772	0.312	QSO (Opt.var.)
11 04 27.1	38 12 32	MRK 421	0.030	BL Lac
11 06 43.5	72 34 07	NGC 3516	0.009	Sy1.5
11 11 31.2	34 52 12	FIRST J111130.8+345203	0.212	BL Lac
11 11 37.2	40 50 31	ABELL 1190:[SBM98]	0.079	GClstr
11 14 22.6	58 23 18	8C 1111+586	0.206	GClstr

The objects of the BSC/NVSS correlation

α	δ	Name	Redshift ^a	Classification ^a
11 17 06.3	20 14 10	87GB 111429.0+203022	0.137 ^C	BL Lac ^C
11 18 03.6	45 06 57	LEDA 139560	0.106	Sy1
11 19 08.1	21 19 15	PG 1116+215	0.176	Sy1
11 20 47.5	42 12 17	1ES 1118+424	0.124	BL Lac
11 21 09.9	53 51 25	1RXS J112109.9+535125	0.103	Sy1
11 23 49.2	72 30 02	1RXS J112349.2+723002		BL Lac ^C
11 23 57.4	21 29 14	[CWH99] 112356.7+2129	0.199	GClstr
11 31 08.9	31 14 09	TON 0580	0.289	QSO
11 31 21.4	33 34 47	1RXS J113121.4+333447	0.220 ^C	G ^C
11 32 22.4	55 58 28	1RXS J113222.4+555828	0.051	GClstr
11 36 26.6	70 09 32	MRK 180	0.046	BL Lac
11 36 29.4	21 35 53	MRK 739b	0.030	Sy1
11 36 30.9	67 37 08	HS 1133+6753	0.135	BL Lac
11 41 16.2	21 56 25	PG 1138+222	0.063	Sy1
11 44 29.9	36 53 14	KUG 1141+371	0.040	Sy1
11 45 09.3	30 47 25	[HB89] 1142+310	0.060	Sy1.5
11 47 54.9	22 05 48	1RXS J114754.9+220548	0.276*	BL Lac*
11 49 30.4	24 39 28	RGB J1149+246	0.402*	BL Lac ^C
11 53 24.4	49 31 09	[HB89] 1150+497	0.334	QSO
11 55 18.9	23 24 32	MCG +04-28-097	0.143	G
11 57 56.1	55 27 17	NGC 3998	0.003	Sy1;LINER
12 03 08.9	44 31 55	NGC 4051	0.002	Sy1.5
12 03 43.3	28 36 02	1RXS J120343.3+283602	0.373	Sy1
12 05 11.7	39 20 43	1RXS J120511.7+392043	0.037	GClstr
12 09 46.0	32 17 03	FIRST J120945.2+321700	0.145	Sy1
12 11 58.1	22 42 36	1RXS J121158.1+224236	0.455*	BL Lac*
12 13 45.2	36 37 55	NGC 4190	0.001	G
12 15 06.7	33 11 30	NGC 4203	0.004	LINER
12 17 52.1	30 07 05	ON 325 / B2 1215+30	0.130	BL Lac
12 18 27.0	29 48 53	NGC 4253	0.013	Sy1.5
12 21 21.7	30 10 41	FBQS J1221+3010	0.182	BL Lac
12 24 54.9	21 22 52	PG 1222+216	0.435	blazar
12 25 12.5	32 13 54	MAPS-NGP O-267-076115	0.059	GClstr
12 26 23.9	32 44 31	NGC 4395:[R97] 12	0.242 ^C	Sy1 ^C
12 30 14.2	25 18 05	MG2 J123013+2517	0.135	BL Lac ^C
12 31 32.5	64 14 20	[HB89] 1229+645	0.164*	BL Lac*
12 32 03.6	20 09 30	MRK 771	0.063	Sy1
12 36 51.1	45 39 07	CGCG 244-033	0.030	Sy1.5
12 36 58.8	63 11 11	ABELL 1576:[HHP90]	0.302	G
12 37 05.6	30 20 02	FIRST J123705.5+302005	0.700	BL Lac ^C
12 37 39.2	62 58 43	[HB89] 1235+632	0.297	BL Lac
12 38 08.3	53 26 04	87GB 123550.3+534219	0.347 ^C	Sy1 ^C
12 39 23.1	41 32 45	FIRST J123922.7+413251		BL Lac*
12 41 41.2	34 40 32	FIRST J124141.3+344031		BL Lac ^C
12 41 44.4	35 03 53	NGC 4619	0.023	Sy1
12 42 11.3	33 17 03	WAS 61	0.044	Sy1
12 43 12.5	36 27 43	TON 0116		BL Lac ^C
12 47 01.3	44 23 25	RGB J1247+443		AGN
12 48 18.9	58 20 31	PG 1246+586		BL Lac ^C
12 50 52.5	41 07 13	MESSIER 94	0.001	LINER
12 53 01.0	38 26 29	FIRST J125300.9+382625	0.372 ^C	BL Lac ^C
12 57 31.7	24 12 46	1ES 1255+244	0.141	BL Lac

The objects of the BSC/NVSS correlation

α	δ	Name	Redshift ^a	Classification ^a
13 02 55.6	50 56 21	1RXS J130255.6+505621	0.688	BL Lac ^C
13 05 52.6	30 54 06	ABELL 1677	0.183	GClstr
13 13 27.2	36 35 42	NGC 5033	0.003	Sy1.9
13 19 57.2	52 35 33	1RXS J131957.2+523533	0.092	Sy
13 20 16.3	33 08 29	1RXS J132016.3+330829	0.036	GClstr
13 22 48.5	54 55 27	1RXS J132248.5+545527	0.064	Sy1
13 24 00.2	57 39 18	87GB 132204.6+575429	0.115	BL Lac
13 25 49.2	59 19 37	ABELL 1744:[HHP90]	0.151	GClstr
13 26 15.0	29 33 32	87GB 132354.7+294853	0.431	BL Lac
13 34 47.5	37 11 00	BH CVn		star (F2IVRSCVn D)
13 35 08.2	20 46 41	1RXS J133508.2+204641		var. K0 star
13 37 18.8	24 23 07	[HB89] 1334+246	0.108	Sy D
13 40 29.9	44 10 07	87GB 133822.3+442514	0.548*	BL Lac ^C
13 41 04.8	39 59 42	B3 1338+402	0.163	BL Lac
13 41 52.6	26 22 30	1RXS J134152.6+262230	0.075	GClstr*
13 45 45.1	53 33 01	87GB 134352.4+534755	0.135*	Sy1 ^C
13 48 52.6	26 35 41	ABELL 1795:[MK91]	0.062	GClstr
13 53 28.2	56 01 02	1RXS J135328.2+560102	0.370	BL Lac
13 54 20.2	32 55 47	UGC 08829	0.026	Sy1
13 55 15.9	56 12 44	1RXS J135515.9+561244	0.122	Sy1
13 55 53.3	38 34 28	MRK 464	0.051	Sy1.5
14 04 50.2	65 54 34	1RXS J140450.2+655434	0.364	BL Lac ^C
14 06 22.2	22 23 50	PG 1404+226	0.098	Sy
14 10 31.6	61 00 20	1RXS J141031.6+610021	0.384	BL Lac ^C
14 13 42.6	43 39 38	MAPS-NGP O-221-004710	0.089	G
14 13 58.3	76 44 56	1RXS J141358.3+764456	0.068*	Sy2*
14 17 56.8	25 43 29	1E 1415+259	0.237	BL Lac
14 17 59.6	25 08 18	SN 1984Z	0.017	SNR in NGC5548
14 21 36.4	49 33 05	MCG +08-26-021	0.072	GClstr
14 21 39.7	37 17 43	1RXS J142139.7+371743	0.160	GClstr
14 22 39.1	58 01 59	RGB J1422+580	0.638	BL Lac ^C
14 23 13.4	50 55 37	87GB 142127.2+510856	0.274	Sy1
14 23 53.6	40 15 33	1RXS J142353.6+401533	0.082	GClstr
14 23 56.0	26 26 30	1RXS J142356.0+262630		Prob. GClstr*
14 26 01.3	37 49 36	ABELL 1914	0.171	GClstr
14 27 00.5	23 48 03	PG 1424+240		BL Lac
14 28 32.6	42 40 28	1ES 1426+428	0.129	BL Lac
14 31 04.8	28 17 16	MRK 684	0.046	Sy1
14 31 06.2	25 38 15	1RXS J143106.2+253815	0.096	GClstr
14 32 36.0	31 38 55	1RXS J143236.0+313855	0.132	GClstr
14 39 17.7	39 32 48	PG 1437+398		BL Lac ^C
14 42 07.7	35 26 32	MRK 478	0.079	Sy1
14 42 18.9	22 18 20	UGC 09480	0.097	GClstr
14 43 02.8	52 01 41	3C 303	0.141	G
14 44 33.9	63 36 04	MS 1443.5+6349	0.299	BL Lac
14 48 01.0	36 08 33	[WB92] 1446+3620		BL Lac
14 49 32.3	27 46 30	RBS 1434	0.228*	BL Lac*
14 51 08.5	27 09 33	PG 1448+273	0.065	Sy1
14 56 03.4	50 48 24	1RXS J145603.4+504824	0.480	BL Lac
14 57 15.4	22 20 26	MS 1455.0+2232	0.258	GClstr
14 58 27.3	48 32 50	1RXS J145827.3+483250	0.539	BL Lac
15 00 20.7	21 22 14	LEDA 140447	0.153	G

The objects of the BSC/NVSS correlation

α	δ	Name	Redshift ^a	Classification ^a
15 01 01.7	22 38 12	MS 1458.8+2249	0.235	BL Lac
15 04 13.1	68 56 10	[HB89] 1503+691	0.318	Sy1
15 07 44.6	51 27 10	MRK 845	0.046	Sy1
15 08 42.2	27 09 10	RBS 1467	0.270*	BL Lac ^C
15 10 40.8	33 35 15	1RXS J151040.8+333515	0.116 ^C	BL Lac ^C
15 14 43.1	36 50 59	[HB89] 1512+370	0.371	QSO/Sy1?
15 17 47.3	65 25 23	1517+656	0.702 ^C	BL Lac ^C
15 21 53.0	20 58 30	1RXS J152153.0+205830		star M9
15 23 46.0	63 39 30	4C +63.22	0.204	G
15 29 07.5	56 16 05	IRAS F15279+5626	0.099	Sy1
15 32 02.3	30 16 31	87GB 152959.0+302636	0.064	BL Lac
15 32 53.7	30 21 03	RBS 1509	0.361	LINER/GClstr
15 33 24.9	34 16 40	87GB 153121.5+342710		BL Lac
15 35 01.1	53 20 42	1ES 1533+535	0.890	BL Lac ^C
15 35 52.0	57 54 04	MRK 290	0.030	Sy1
15 39 50.3	30 43 05	1RXS J153950.3+304305	0.097	GClstr
15 40 16.4	81 55 05	1ES 1544+820		BL Lac ^C
15 47 44.2	20 51 56	3C 323.1	0.264	QSO
15 54 24.3	20 11 16	MS 1552.1+2020	0.222	BL Lac
15 58 18.7	25 51 18	MRK 864	0.072	Sy2
15 59 09.5	35 01 45	UGC 10120	0.031	Sy1

(continued on the next page)

^a new entries first presented here marked with *, confirmed identifications/redshifts: ^C

Table 9. The HRX-BL Lac sample

Name ^a	α	δ	z^b	f_X^c	f_R^d	B mag ^e	K mag	Ca break
1RXS J071030.0+590808	07 10 30.1	+59 08 20	0.125	10.15	159.2	18.4		
1RXS J071218.9+571948*	07 12 18.9	+57 19 48	0.095	1.01	7.9	20.1		34%
0716+714	07 21 53.5	+71 20 36		1.26	727.2	15.5	10.4	
MS 0737.9+7441	07 44 05.1	+74 33 58	0.0311	4.46	23.3	16.9	14.6	
1RXS J074929.4+745142	07 49 29.7	+74 51 45	0.605	2.80	44.8	18.9	15.2	2%
1RXS J080323.1+481622* <i>new</i>	08 03 22.9	+48 16 19	0.503	0.92	12.6	18.8		5%
1RXS J080525.8+753424	08 05 26.9	+75 34 25	0.121	2.59	52.6	18.1	13.7	
1RXS J080625.5+593105	08 06 25.9	+59 31 06		2.06	60.9	17.9		
1RXS J080938.5+345544	08 09 38.5	+34 55 37	0.082	2.62	223.4	17.0	14.5	
1RXS J080949.2+521855	08 09 49.0	+52 18 56	0.138	4.71	182.8	15.6		
1RXS J081624.6+573910* <i>new</i>	08 16 22.7	+57 39 09		0.94	100.0	18.8		5%
1RXS J083251.9+330011	08 32 52.0	+33 00 11	0.671	1.25	6.6	20.7		
1RXS J083357.5+472658* <i>new</i>	08 33 57.1	+47 26 51	0.496	0.82	11.6	19.7		14%
1RXS J085407.7+440840* <i>new</i>	08 54 09.8	+44 08 31		0.76	79.8	18.5	14.3	
1RXS J085451.0+621843* <i>new</i>	08 54 50.5	+62 18 50	0.267?	0.83	387.6	19.0		
1RXS J085916.5+834450	08 59 10.1	+83 45 04	0.327	1.23	10.2	19.7 ¹		9%
1RXS J090315.3+405609*	09 03 14.7	+40 56 01	0.190	0.93	38.2	19.3		25%
B2 0906+31	09 09 53.3	+31 06 02	0.274	2.18	195.5	18.3	14.1	3%
1RXS J091324.6+813318	09 13 20.4	+81 33 06	0.639	2.28	4.9	20.7 ¹		5%
B2 0912+29	09 15 52.2	+29 33 20		3.36	342.0	16.3 ¹	12.7	
1RXS J091651.8+523829	09 16 52.0	+52 38 27	0.190	2.02	138.9	18.3 ¹	14.3	
1RXS J092401.1+053350* <i>new</i>	09 24 01.1	+05 33 50		1.34	7.5	19.6 ¹		
1RXS J092804.2+744714	09 28 03.0	+74 47 19	0.638	1.13	85.8	20.8 ¹		
1ES 0927+500	09 30 37.6	+49 50 24	0.186	13.45	21.4	18.0		26%
1RXS J093056.2+393332*	09 30 56.9	+39 33 37	0.641	0.80	13.0	19.5		30%

The HRX-BL Lac sample

Name ^a	α	δ	z^b	f_X^c	f_R^d	B mag ^e	K mag	Ca break
1RXS J094020.7+614837* <i>new</i>	09 40 22.5	+61 48 25	0.212	0.85	12.8	18.4		29%
1RXS J095214.4+393627* <i>new</i>	09 52 14.0	+39 36 08		0.65	3.0	19.8	15.7	
1RXS J095225.8+750216	09 52 23.8	+75 02 13	0.178	1.98	12.2	19.3 ¹	14.6	
1RXS J095410.8+491457*	09 54 09.8	+49 14 59	0.207	0.76	2.7	19.3		
1RXS J095929.8+212340	09 59 30.0	+21 23 19	0.367	2.32	40.8	19.1 ¹	14.6	3%
1RXS J100656.9+345446* <i>new</i>	10 06 56.3	+34 54 44	0.612?	0.66	6.6	18.7		-14%
1RXS J100811.5+470526	10 08 11.4	+47 05 20	0.343	4.37	4.7	19.9 ¹		
1RXS J101244.4+422959	10 12 44.2	+42 29 57	0.376	3.86	79.5	18.4 ¹	14.9	-2%
GB 1011+496	10 15 04.0	+49 25 59	0.200	6.78	378.1	16.5	13.1	
1RXS J101616.4+410817	10 16 16.8	+41 08 12	0.281	2.50	14.8	19.5 ¹	14.6	
MS 1019.0+5139	10 22 11.3	+51 24 15	0.141	3.35	5.1	18.0		
1ES 1028+511	10 31 18.6	+50 53 34	0.361	18.02	37.9	16.8	13.9	
1RXS J103744.9+571159*	10 37 44.3	+57 11 56		0.60	71.7	16.7		
1RXS J104148.9+390133* <i>new</i>	10 41 49.0	+39 01 22	0.210	0.71	33.9	18.5	14.4	28%
1RXS J105125.1+394329	10 51 25.4	+39 43 26	0.498	1.67	10.8	19.0 ¹	15.4	-1%
1RXS J105607.0+025215*	10 56 06.3	+02 52 28	0.235	6.18	4.3	19.4 ¹		
1RXS J105723.5+230317	10 57 23.0	+23 03 15	0.378	2.14	7.9	19.7 ¹		13%
1RXS J105837.5+562816	10 58 37.8	+56 28 09	0.144	1.36	228.5	15.8		
1RXS J110021.3+401933	11 00 21.0	+40 19 29	0.225?	2.21	18.3	18.6 ¹	15.2	-5%
MRK 421	11 04 27.3	+38 12 32	0.030	116.48	768.5	13.3		
1RXS J110748.2+150217* <i>new</i>	11 07 48.2	+15 02 17		2.17	43.5	18.4 ¹	14.8	
1RXS J111131.2+345212	11 11 30.9	+34 52 01	0.212	2.73	8.4	19.7 ¹		
1RXS J111706.3+201410	11 17 06.3	+20 14 08	0.137	24.01	103.1	16.0	12.4	-12%
1ES 1118+424	11 20 48.1	+42 12 12	0.124	4.63	24.1	18.0 ¹	14.7	
1RXS J112349.2+723002	11 23 49.2	+72 30 18		1.89	12.5	18.6	13.6	
MRK 180	11 36 26.6	+70 09 25	0.046	19.73	328.4	14.7	12.4	
HS 1133+6753	11 36 30.3	+67 37 05	0.135	11.40	45.8	17.6	13.8	
1RXS J114754.9+220548	11 47 54.9	+22 05 34	0.276	1.39	4.1	21.0	15.0	33%
1RXS J114930.4+243928	11 49 30.3	+24 39 27	0.402	2.56	28.5	19.0 ¹		5%
1RXS J121158.1+224236	12 11 58.7	+22 42 32	0.455	2.61	20.2	19.6 ¹		7%
ON 325 / B2 1215+30	12 17 52.0	+30 07 02	0.130	11.79	572.7	15.6	12.0	
PG 1218+304	12 21 21.8	+30 10 37	0.182	9.14	71.5	17.7	13.3	
ON 231* / W Comae*	12 21 31.7	+28 13 58	0.102	1.00	732.1	16.5		
1RXS J122424.2+243618*	12 24 24.2	+24 36 24	0.218	0.96	25.9	17.7	13.7	
1RXS J123014.2+251805	12 30 14.0	+25 18 07	0.135	1.34	244.0	16.0 ¹	11.7	
MS 1229.2+6430	12 31 31.5	+64 14 16	0.164	1.97	58.8	18.0 ¹	13.8	
1RXS J123144.7+284754* <i>new</i>	12 31 43.9	+28 47 51	0.236	0.83	141.5	17.5	14.6	-2%
1RXS J123705.6+302002	12 37 06.0	+30 20 05	0.700	3.23	5.6	20.0		
MS 1235.4+6315	12 37 39.1	+62 58 41	0.297	1.62	12.5	18.9 ¹	14.7	
1RXS J123923.1+413245	12 39 22.7	+41 32 52	0.16?	1.17	9.1	20.3 ¹		
1RXS J124141.2+344032	12 41 41.4	+34 40 31		1.06	10.2	20.2 ¹		
1RXS J124312.5+362743	12 43 12.7	+36 27 45		4.66	147.9	16.6 ¹	13.4	
1RXS J124818.9+582031	12 48 18.8	+58 20 29		1.73	245.3	14.9 ¹	12.0	
1RXS J125301.0+382629	12 53 00.9	+38 26 26	0.372	4.38	4.8	18.9 ¹		
1ES 1255+244	12 57 31.9	+24 12 40	0.141	4.76	14.7	15.4		
1RXS J130255.6+505621	13 02 58.0	+50 56 18	0.688	2.79	2.8	19.3 ¹		
1RXS J132400.2+573918	13 24 00.0	+57 39 16	0.115	1.11	44.2	17.8 ¹	13.5	
1RXS J132615.0+293332	13 26 15.0	+29 33 30	0.431	1.48	5.6	18.7 ¹		
1RXS J134029.9+441007	13 40 29.5	+44 10 07	0.548	1.91	57.2	19.3 ¹	15.0	-1%
1RXS J134104.8+395942	13 41 04.9	+39 59 35	0.163	3.83	88.8	18.6 ¹	14.3	
1RXS J134551.8+425747*	13 45 55.3	+36 50 14	0.255	0.41	144.8	20.3	14.6	34%
1RXS J135328.2+560102	13 53 28.0	+56 00 55	0.370	1.31	14.9	19.1 ¹	15.5	

The HRX-BL Lac sample

Name ^a	α	δ	z^b	f_X^c	f_R^d	B mag ^e	K mag	Ca break
1RXS J140450.2+655433	14 04 49.6	+65 54 30	0.364	1.07	15.4	19.4 ¹	15.0	
1RXS J141031.6+610020	14 10 31.7	+61 00 10	0.384	1.37	11.4	19.9 ¹	15.4	
1E 1415+259	14 17 56.6	+25 43 25	0.237	10.43	89.6	16.0	13.9	
1RXS J141946.4+542324*	14 19 46.6	+54 23 15	0.151	0.64	788.7	15.7	12.4	
1RXS J142239.1+580159	14 22 39.0	+58 01 55	0.638	10.03	13.2	17.9 ¹		
1RXS J142422.9+343407* <i>new</i>	14 24 22.7	+34 33 57	0.571?	0.80	10.0	18.3		
1RXS J142700.5+234803	14 27 00.5	+23 48 03		2.04	430.1	16.4		
1ES 1426+428	14 28 32.6	+42 40 21	0.129	21.75	58.8	16.5	13.6	
1RXS J143658.7+563934* <i>new</i>	14 36 57.8	+56 39 25		1.01	21.3	18.8		
1RXS J143917.7+393248	14 39 17.5	+39 32 43		5.12	42.8	16.0	13.7	
MS 1443.5+6349	14 44 34.9	+63 36 06	0.299	1.07	18.9	19.7 ¹	15.3	
1RXS J144801.0+360833	14 48 01.0	+36 08 33		1.55	36.2	17.2	13.7	
1RXS J144932.3+274630	14 49 32.7	+27 46 22	0.228	3.56	90.7	20.0 ¹	14.6	15%
1RXS J145127.5+635421*	14 51 26.0	+63 54 24	0.650	0.90	10.0	19.6		
1RXS J145603.4+504824	14 56 03.7	+50 48 25	0.480	8.60	4.0	18.6 ¹		
1RXS J145827.3+483250	14 58 28.0	+48 32 40	0.539	2.68	3.1	20.4 ¹		
1RXS J150101.7+223812	15 01 01.9	+22 38 06	0.235	2.06	32.4	15.5 ¹		
1RXS J150842.2+270910	15 08 42.7	+27 09 09	0.270	2.99	39.9	18.8 ¹		6%
1RXS J151040.8+333515	15 10 42.0	+33 35 09	0.116	1.74	8.8	18.5 ¹	13.8	37%
1ES 1517+656	15 17 47.5	+65 25 24	0.702	8.03	37.7	16.9 ¹	13.6	
1RXS J153202.3+301631	15 32 02.2	+30 16 29	0.064	2.71	54.4	15.5		
1RXS J153324.9+341640	15 33 24.3	+34 16 40		1.32	30.0	17.9		
1ES 1533+5320	15 35 00.8	+53 20 35	0.890?	8.03	18.2	18.9 ¹		
1RXS J153528.7+392242*	15 35 29.1	+39 22 47	0.257	0.07	19.7	19.8	14.6	
1ES 1544+820	15 40 15.7	+81 55 06		4.02	69.9	17.1 ¹	14.2	
1RXS J155411.8+241415* <i>new</i>	15 54 11.9	+24 14 28	0.301	0.95	12.7	20.4 ¹		13%
MS 1552.1+2020	15 54 24.1	+20 11 25	0.222	2.40	79.4	18.5 ¹		

^a objects not included in the *complete sample* marked with an asterisk, new identifications marked with *new*

^b uncertain redshifts are marked with an “?”

^c ROSAT PSPC (0.5 - 2.0 keV) flux in $10^{-12}\text{erg cm}^{-2}\text{sec}^{-1}$

^d radio flux at 1.4 GHz in mJy

^e B magnitudes determined with the Calar Alto 1.23m telescope are marked with ¹

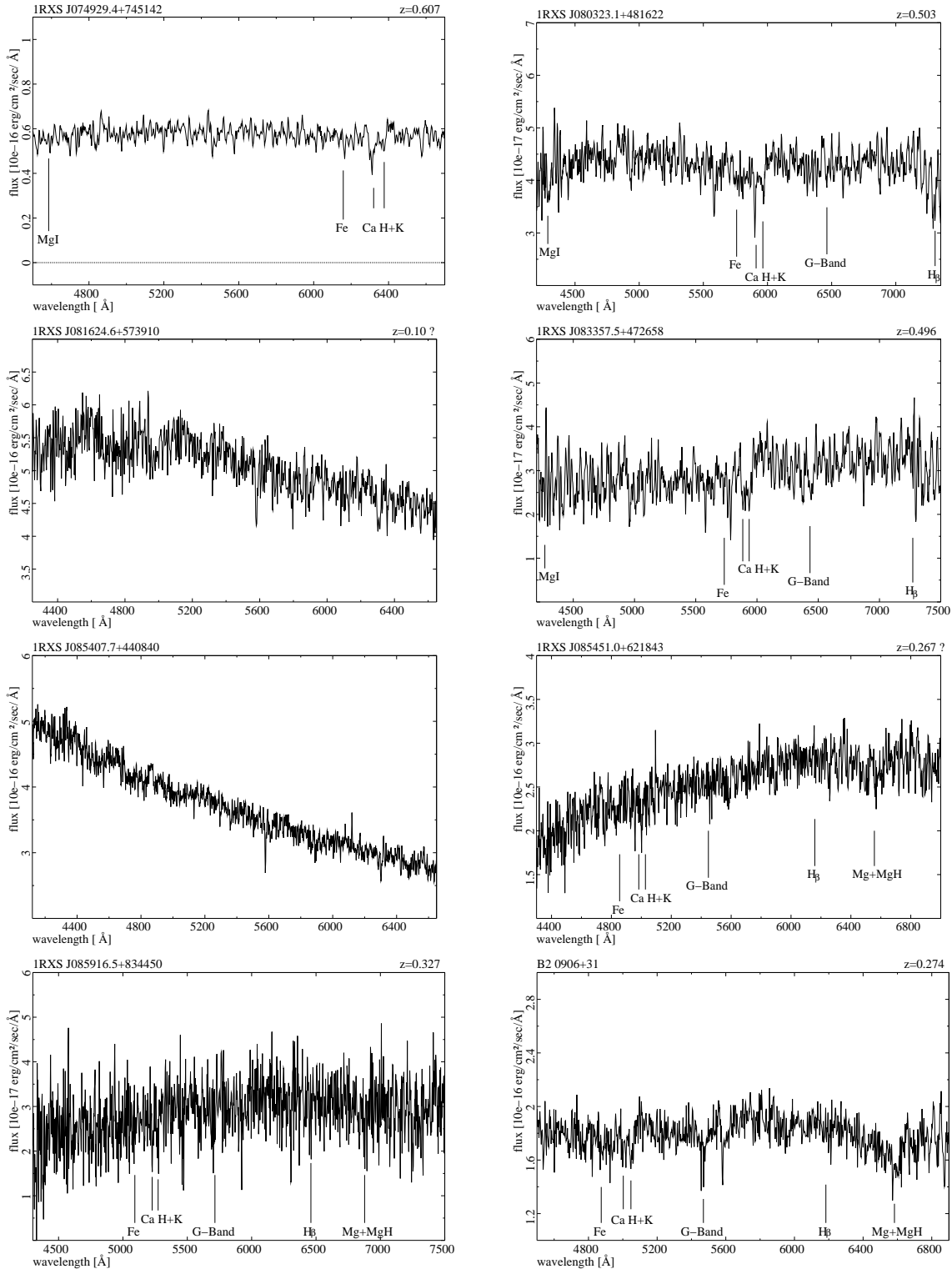


Fig. 8. Optical spectra of new BL Lac objects and of BL Lacs with newly determined redshifts.

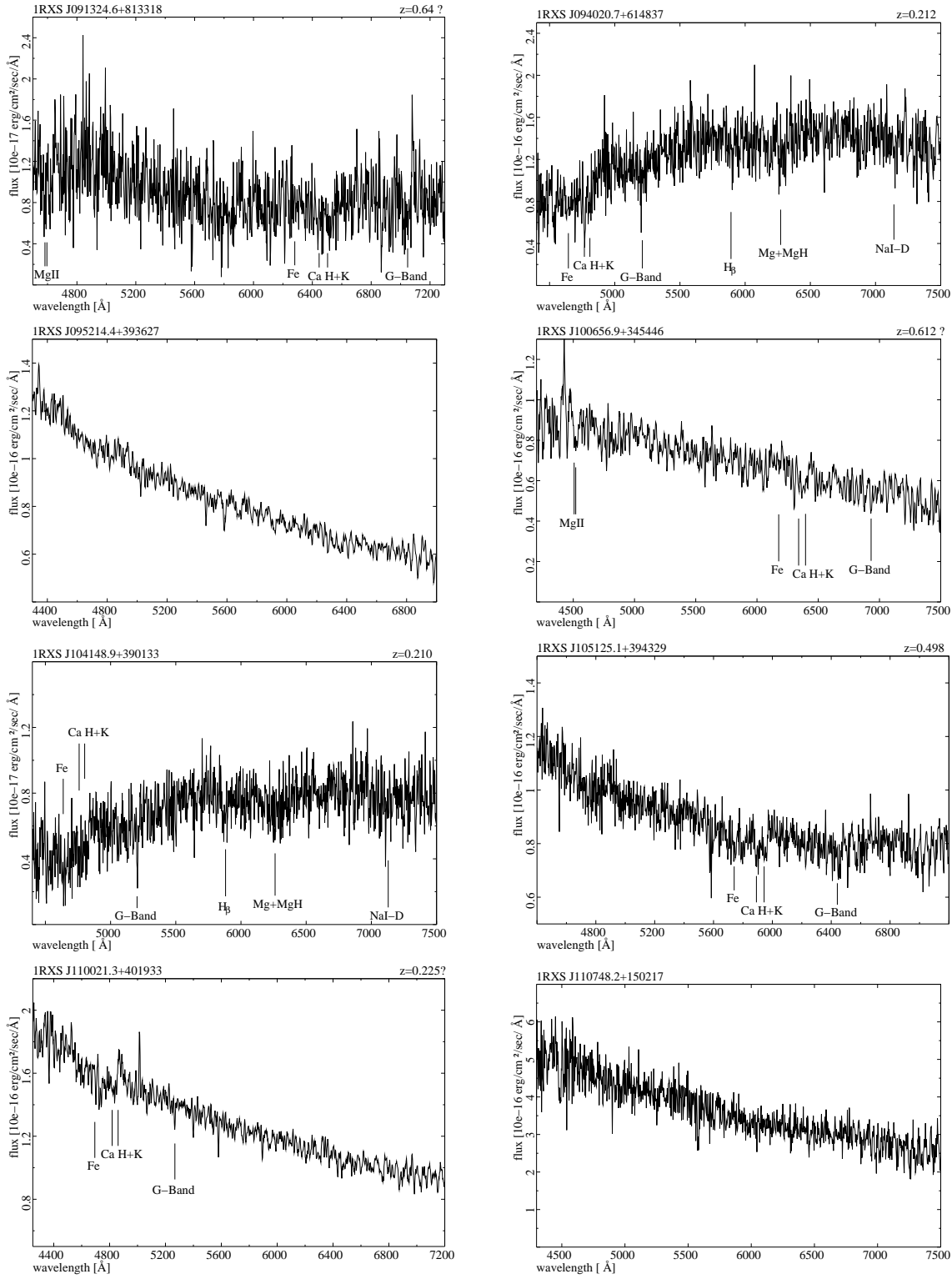


Fig. 8. Optical spectra of new BL Lac objects and of BL Lacs with newly determined redshifts.

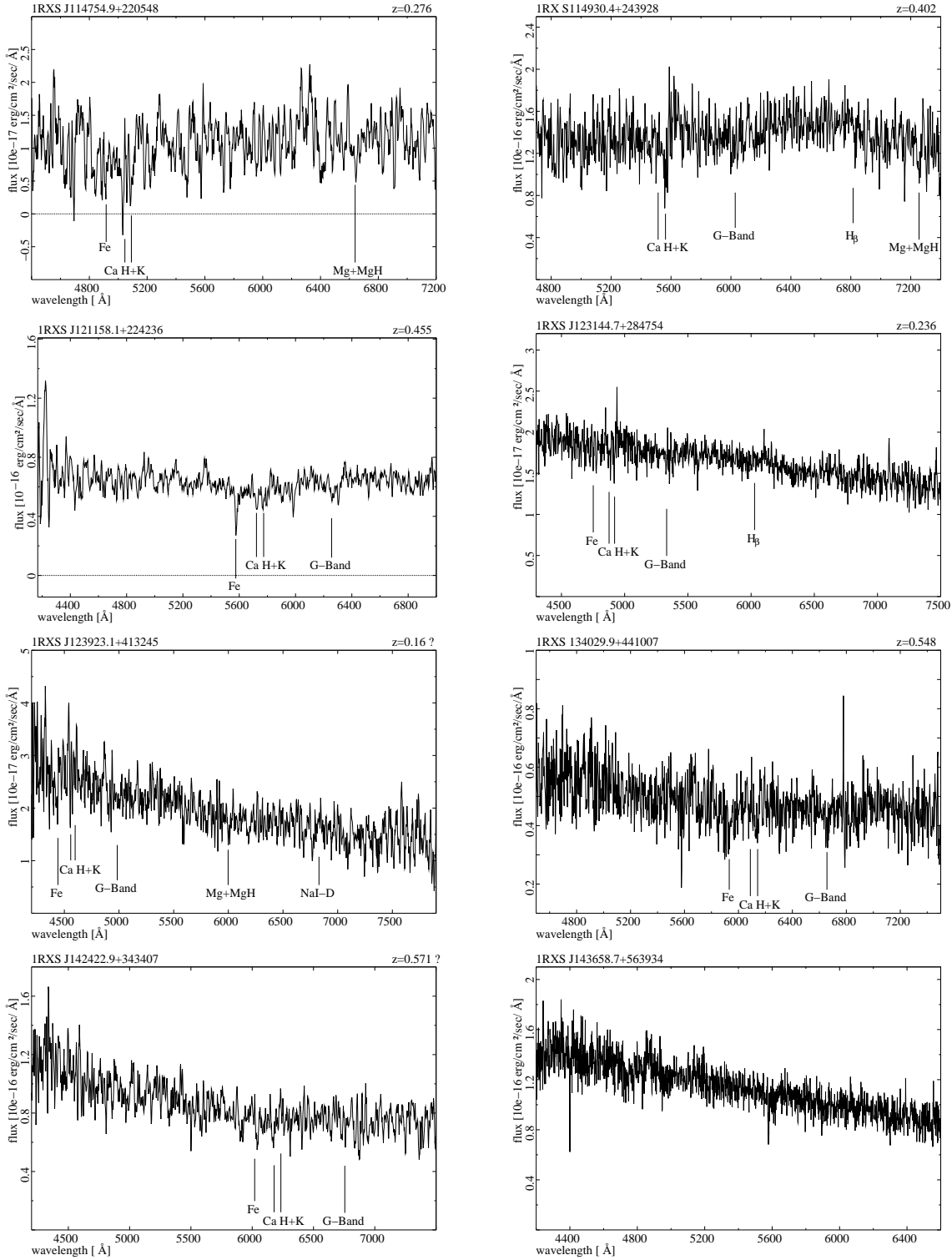


Fig. 8. Optical spectra of new BL Lac objects and of BL Lacs with newly determined redshifts.

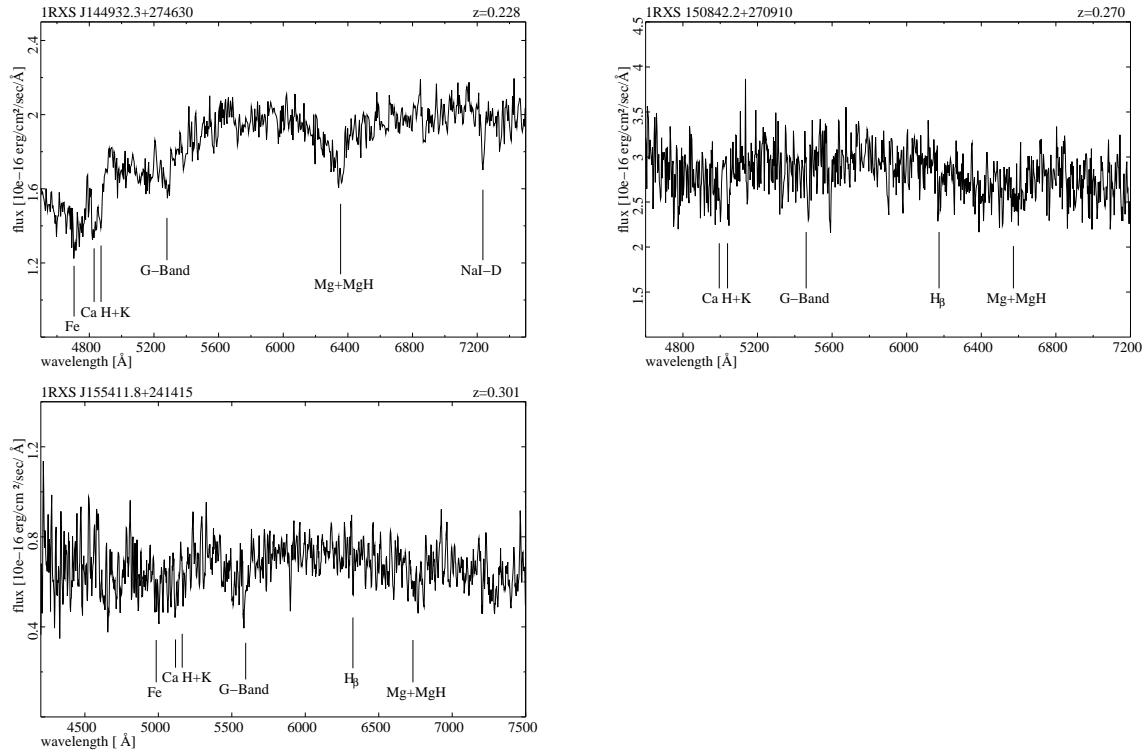


Fig. 8. Optical spectra of new BL Lac objects and of BL Lacs with newly determined redshifts.